Journal of Hard Tissue Biology 16[3] (2007) p143-145

CODEN-JHTBFF, ISSN 1341-7649

Short Communication

Analysis of Liquid Specimen in a Glass Ampoule by 532 nm Laser Micro-FT-Raman

Toshiro Sakae[1,2], Yasuko Numata[3], Hiroyuki Okada[4], Isamu Sato[5], and Makoto Otsuka[2]

[1] Department of Anatomy, Nihon University School of Dentistry at Matsudo, Chiba, 271-8587, Japan
[2] Department of Pharmaceutical Technology, Research Institute of Pharmaceutical Sciences, Musashino University, Shinmachi 1-1-20, Nishi-Tokyo, 202-8585, Japan
[3] Department of Prosthodontics, Nihon University School of Dentistry at Matsudo, Chiba, 271-8587, Japan
[4] Department of Oral Pathology, Nihon University School of Dentistry at Matsudo, Chiba, 271-8587, Japan
[5] Advanced Research Institute for the Sciences and Humanities, Nihon University, Tokyo, 102-8251, Japan
(Accepted for publication, October 24, 2007)

Abstract: Micro FT-Raman spectroscopy was applied to examine the contents in a glass ampoule non-destructively. Water, linger solution, ethanol and nail color remover liquid were examined. Glass was sufficiently thin enough to obtain Raman spectrum from the contents in the ampoule. All the examined materials showed the fine Raman profiles. The results indicated that micro-FT-Raman has a potential to examine and check the contents and impurities in the ampoule non-destructively.

Key Words: Micro FT-Raman, Glass ampoule, Liquid, Alcohol, Acetone

Introduction

Glass ampoule is widely used for clinical trials under taken care of the guidance such as the Center for Drug Evaluation and Research (CDER), and/or the Center for Biologistics Evaluation and Research (CBER) (1). These medical use ampoules are very carefully manufactured, but in rare cases they contained impurities such as fragments of glasses, metals, insects, etc. Some efforts are taken to understand and not only qualify but also quantify the impurities in drugs and medicines (2). To analyze the content of glass ampoule in intact is a matter of challenge and some fine-art techniques are introduced (3). Among many non-destructive analytical methods, micro FT-IR spectroscopic method is one of the most popular methods for the ease of handle of specimen and instrument as well as analytical cost. However, FT-IR analysis of liquid specimen requires some special expensive attachments and techniques. FT-Raman had a great improvement in the last decay, and has an extreme potential to analyze the materials in any phases including solid, gasses and liquid. Micro-Raman is a conventional analytical instrument which is equipped with a microscope and able to analyze pointed regions with a few mm sizes. In this study, a micro-FT-Raman spectroscopy was applied to detect the content in a glass ampoule.

Corresponding author: Toshiro Sakae phD,Department of Histology, Embryology and Anatomy,Nihon University School of Dentistry at Matsudo,Chiba, 271-8587, Japan Phone:+81-47-360-9323, Fax:+81-47-360-9323,E-mail: sakae.toshiro@nihon-u.ac.jp

Materials and Methods

Materials

A standard brownish glass ampoule was used as a container of the tested liquids: pure water, pure ethanol and nail color remover (Bersante Co. Ltd.). The glass ampoules was filled with each liquid and examined using a micro-FT-Raman described below.

Micro FT-Raman Spectroscopy

Micro FT-Raman study was carried out using a RXN system, Kaiser Optical Systems Inc., USA, equipped with an OLYMPUS BX51 TRF microscope. Micro-Raman spectra were acquired with a Kaiser RXN1 Fourier transform Raman (FT Raman) spectrometer. The green laser source was a NewPort INVICTUS operated at 532 nm. An iDUS, ANDOR Technology, thermoelectric cooled CCD was used for detection. Rayleigh line rejection was accomplished with a HoloPlex transmissive grading, Kaiser and spectra for this work were acquired over the range of 100-4400-cm^{-1} Raman shift. All Raman spectra were acquired as at 2.5 cm^{-1} resolution. Data acquisition was carried under the conditions of the accumulation time: 2 sec. and the accumulation number: 2. To reduce fluorescence arising from the glass ampoule (brown cylindrical, ~18-mm o.d.), the laser was focused 1-2 mm inside the ampoule.

Results

Fig. 1 showed the micro FT-Raman spectra of the glass of the

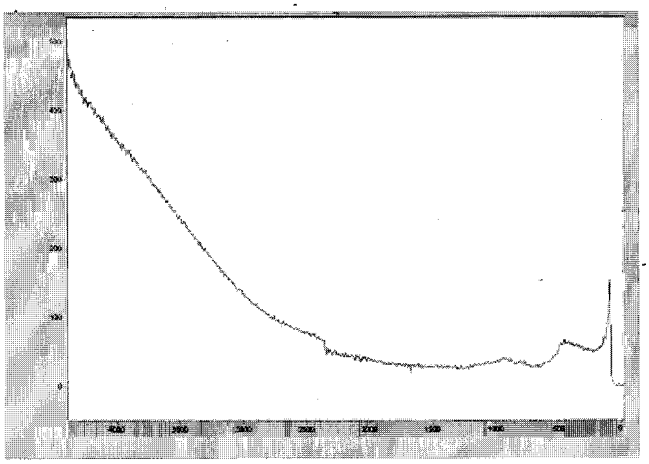

Fig.1. Micro FT-Raman spectra of the ampoule glass tube.

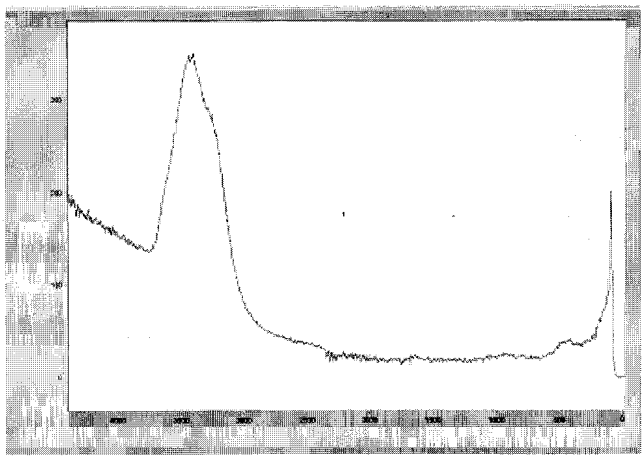

Fig. 2. Micro FT-Raman spectra of water in the ampoule.

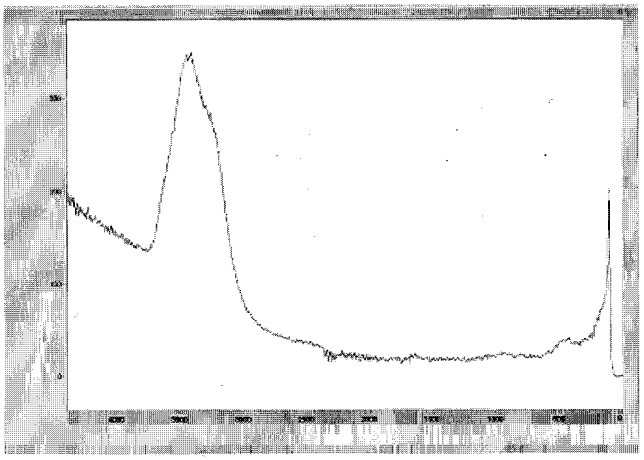

Fig. 3. Micro FT-Raman spectra of linger liquid in the ampoule.

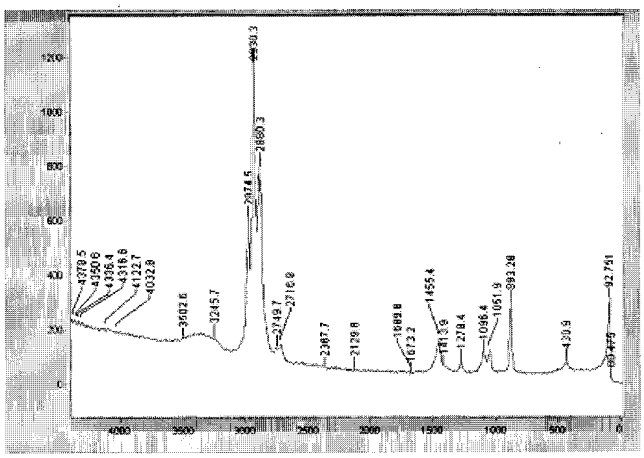

Fig. 4. Micro FT-Raman spectra of ethanol in the ampoule.

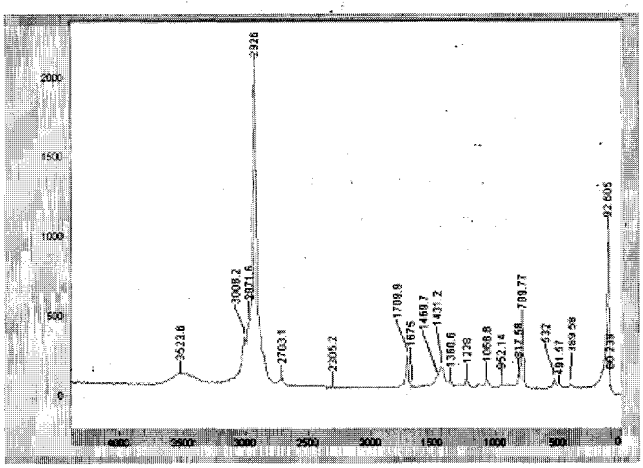

Fig. 5. Micro FT-Raman spectra of nail-remover liquid in the ampoule.

ampoule. As expected, FT-Raman spectra of the glass did not show any significant Raman shift in the range between 100 cm^{-1} and 4400 cm^{-1}. Two types of glass ampoule were tested by the micro FT-Raman: one made of transparent glass ampoule and the other made of brown colored gall ampoule. There was no significant difference between them in Raman spectra.

Fig. 2 showed the micro FT-Raman spectra of water in the ampoule. There was no significant peak but a strong broad peak at around 3000-3500 cm^{-1} due to water molecules.

Fig. 3 showed the micro FT-Raman spectra of Linger solution in the ampoule. The spectra of Linger solution was almost the same to that of water.

Fig. 4 and Fig. 5 showed the micro FT-Raman spectra of ethanol and nail color remover liquid in the ampoule respectively. The Raman peaks of ethanol and the nail color remover were clearly differentiated from each other as listed in Table 1 together with the ethanol (4) and acetone (5) data.

Discussion

This study showed that FT-Raman spectroscopic analysis is a powerful tool for examination of contents in a glass ampoule. The glass did not affect the obtained Raman spectra in peak shift and intensity. The two examined organic solvents were clearly differentiated. The tested ethanol (C_2H_6O) showed identical Raman peaks to the reference data (4). The nail color remover used in this study contained acetone (C_3H_6O), water (H_2O), polyethylene glycol (HO-(CH_2-CH_2-O)$_n$-H (PEG-12)), isopropanol or isopropyl

Table 1. Three strong Raman peaks were marked by **BOLD** type.

Water	Ethanol	Nail remover	Ethanol (ref. lingj23864)	Acetone (ref. Acetone)
cm-1	cm-1	cm-1	cm-1	
3500-3000	3500-3200	3524		
		3008		3006
	2975	2972		2968
	2930	**2926**	2931	2924
	2880			2848
	2749			
	2717	2703		2698
		2305		
		1710		1710
	1455	1431	1453	1428
	1414			
		1361		1356
	1278		1274	
		1228		1222
	1096		1097	
	1052	1069	1051	1066
	883		883	
		790		788
		532		530
		492		
	431		431	
		390		394

alcohol ($CH_3CH(OH)CH_3$), campher ($C_{10}H_{16}O$), some perfumes and others, including aloe extract. The Raman spectra obtained for the nail color remover was identified with acetone in majorty as shown in Table 1.

Raman spectrometry is, as well as FT-IR, able not only to identify components but also to quantify the amount of each component, although they are in minor content. Micro FT-Raman has many advantages over micro FT-IR such as a pin-point detection as small as 1 mm in size. However, there are several problems to be sold, e.g., self-fluorescence from organic matters which rise background and disappear the essential peaks.

Acknowledgements

Micro FT-Raman spectrometer used in this study was equipped at LEBRA, Nihon University. The authors thank to the members of LEBRA for their support. This study was supported by a Grant-in-Aid for Scientific Research (No. 17591927) from JSPS, Japan, and the Frontier Science Projects to LEBRA, 2000 and 2005 from MEXT, Japan.

References

1. CDER Guidance Document: Guidance for Industry Q1A Stability Testing of New Drug Substances and Products. U.S. Department of Health and Human Services, Food and Drug Administration, Center for Drug Evaluation and Research (CDER), Center for Biologics Evaluation and Research (CBER), ICH, Revision 1; August 2001
2. Roy J.: Pharmaceutical Impurities- A Mini-Review. AAPS Pharm Sci Tech. 3(2):article 6, 2002
3. Christesen S, Maciver B, Procell L, Sorrick D, Carrabba M, and Bello J.: "Nonintrusive Analysis of Chemical Agent Identification Sets Using a Portable Fiber-Optic Raman Spectrometer," Appl. Spectrosc 53, 850-855, 1999
4. Ling J.: The development of Raman imaging microscopy to visualize drug actions in living cells. Ph.D. thesis, Univ. of Texas at Austin, 2001
5. UTIL191: Raman database, University Bpclermont, France.
6. Sakae T, and Davies JE.: Infrared spectroscopic method for analysis of precipitates on a cell culture dish. J Biol Buccale 20(2):129-133, 1992

Lasers Med Sci (2007) 22: 15–20
DOI 10.1007/s10103-006-0414-x

ORIGINAL ARTICLE

Toshiro Sakae · Yukie Sato · Yasuko Numata · Taketoshi Suwa · Tohru Hayakawa · Kunihiro Suzuki · Takao Kuwada · Ken Hayakawa · Yasushi Hayakawa · Toshinari Tanaka · Isamu Sato

Thermal ablation of FEL irradiation using gypsum as an indicator

Received: 18 August 2006 / Accepted: 20 September 2006 / Published online: 15 November 2006

Abstract Thermal effects produced in a laser-irradiated sample were studied by micro-X-ray diffraction and micro-Fourier transform infrared spectroscopy (FTIR). Gypsum, transformed into bassanite at 124°C and into anhydrite at 147°C, was used as a thermal indicator. Pit formation by a wavelength-tunable free electron laser (FEL) irradiation on the gypsum pellet maximized at a wavelength of 3.0 μm, 2 mJ/shot, and pits were not detected in those irradiated at 2.6 or 3.8 μm compared with the maximum at 3.0 μm and diminished at 2.0 or 4.0 μm in the human tooth case. Micro-X-ray diffraction and micro-FTIR did not reveal any appreciable bassanite or anhydrite in the irradiated regions. From the laser ablation viewpoint, these results allow the FEL ablation to be considered as plasma or evaporative ones. This study indicated that the micro-pulse of laser was effective to prevent thermal damages of laser irradiation.

T. Sakae (✉) · K. Suzuki
Department of Anatomy, Nihon University School of Dentistry, Matsudo, Chiba 271-8587, Japan
e-mail: sakae.toshiro@nihon-u.ac.jp
Tel.: +81-47-3609323
Fax: +81-47-3609323

Y. Sato
Department of Oral Pathology, Nihon University School of Dentistry, Matsudo, Chiba 271-8587, Japan

Y. Numata · T. Suwa
Department of Prosthodontics, Nihon University School of Dentistry, Matsudo, Chiba 271-8587, Japan

T. Hayakawa
Department of Dental Biomaterials, Nihon University School of Dentistry, Matsudo, Chiba 271-8587, Japan

T. Sakae · T. Kuwada · K. Hayakawa · Y. Hayakawa · T. Tanaka · I. Sato
LEBRA, Laboratory for Electron Beam Research and Application, Institute of Quantum Science, Nihon University, Funabashi, Chiba 274-8501, Japan

Keywords FEL · Ablation · Anhydrite · Hemihydrate · Thermal effects

Introduction

The laser wavelength generally selected for laser excavation of dental enamel and dentin, which will replace conventional dental drilling, is 2.94 μm of the Er:YAG laser. Water in tissue has a maximum absorbance at a wavelength of 3.00 μm; hence, it is generally considered that this wavelength is the most destructive to tissues [1]. In previous studies, it was found that laser ablation of dental hard tissues resulted in some thermal modification of their crystalline structure [2–9]. By comparing with heating studies of dental enamel [10–12], it was shown that laser irradiation of dental enamel produced temperature rises of up to 1,600°C [13]. For some clinical applications, it is desirable to avoid these thermal effects produced by laser irradiation. The ablation effects of laser irradiation are usually grouped into the following stages: heating, melting, evaporating and plasma shielding. These ablation effects are strongly dependent upon laser power or fluence, wavelength and pulse structure. The types of lasers generally used in clinical applications and academic research are solid-state lasers, excimer lasers and gas lasers, all of which have fixed wavelength and pulse structure output. Using Q-switching greatly reduces thermal damage. Free electron laser (FEL) is not a conventional laser but is an ideal laser source having ultra-short pulses, high powers and tunable wavelengths. The characteristics of FEL are concisely summarized as follows: FELs produce tunable, coherent, high-power radiation. The wavelength range currently goes from millimeter to visible wavelengths. The radiation emitted from FEL has many characteristics, including high spatial coherency. The FEL located at the Laboratory for Electron Beam Research and Application, Nihon University (referred to hereafter as LEBRA-FEL) has these characteristics of FEL. The free-electron beam is generated by a linear accelerator (LINAC), and it produces 20-μs macro-

pulses having a micro-pulse structure of less than 3 ps. Several pilot studies using FEL have been carried out to ablate various materials [14–25]. In contrast with these studies, irradiation of human dental tissue by LEBRA-FEL did not show any evidence of scorching, either macroscopic or microscopic, although human dental enamel and dentin were effectively etched at a wavelength of 2.94 μm [26]. In this study, gypsum, the thermal properties of which are well known, was irradiated to determine the thermal effect of the wavelength-tunable LEBRA-FEL.

Materials and methods

Reagent-grade crystalline calcium sulfate dehydrate (Wako) was used in this study. The samples were confirmed to be pure gypsum by X-ray diffraction (XRD) and Fourier transform infrared spectroscopy (FTIR). Pellets of gypsum were produced using a hand-press tool usually used for sample preparation in infrared absorption analysis. The pellets were 5.0 mm in diameter and 0.5–1.0 mm in thickness. Three pellets were irradiated at each wavelength (2.6, 3.0 and 3.8 μm).

Human tooth sections were made using the pooled samples in 10% neutral formaldehyde solution. Following a routine tooth sectioning, tooth was cut off by a low-speed diamond saw (Buhler) and then polished by polishing stones.

The thermal properties of the gypsum used in this study were checked using a differential thermal analyzer equipped with a thermogravimeter (DTG-8200, Rigaku, Tokyo) and a differential scanning calorimeter (DSC-8230, Rigaku). The differential thermoanalysis and thermogravimetric (DTA–TA) measurements were carried out under the following conditions: heating range at room temperature, 1,073 K; heating rate, 4–40 K/min; sample weight, about 10–20 mg; TG sensitivity, 0.01 mg; reference material, alpha-alumina and atmosphere, air. The DSC measurement conditions were as follows: sample weight, about 5–10 mg; heating rate, 2–20 K/min; reference material, alpha-alumina and atmosphere, air. The obtained data were analyzed using Rigaku TP2 software.

For LEBRA-LINAC, conditions were as follows: accelerating voltage, 80 MeV; current, 70 mA; macro-pulse, 20 μs, 2 Hz; micro-pulse, about 3 ps at 350-ps intervals and FEL wavelength, 1.0–6.0 μm. The tuned FEL wavelength fluctuation was less than 10 nm. The generation and conditions of LEBRA-FEL are described in [27, 28]. The irradiation energy was regulated by a diaphragm placed in the laser beam and monitored by a power meter using a beam splitter to divert 20% of the laser power. The measured power was used to calculate the power on the sample surface; the measurement error was assumed to be less than 10%. The FEL irradiation was focused on the sample plane using a CaF_2 lens. The LEBRA-FEL irradiation system is described in [26]. The spot position and the number of laser shots were controlled by computer.

The laser-irradiated teeth samples were observed using a binocular microscope (SMZ1500, Nikon, Tokyo). The images were taken using a digital camera and stored. The size and depth of the pits formed by laser irradiation were measured using a surface profilometer (VF-7500, Keyence, Osaka). The measurement error was assumed to be less than 10%.

The irradiated and non-irradiated gypsum pellets were analyzed by micro-XRD (RINT-2500 PSPC, Rigaku) under the following conditions: X-ray generator, rotary-type Cu target; accelerating voltage, 60 kV; accelerating current, 300 mA; X-ray beam collimator, 30 μm in diameter; sample position, 20° to the incident beam (i.e. X-ray irradiation was over an area having a diameter of about 100 μm in the sample plane); sample movement, in sample sway and rotation modes with rocking at 30° about the sample holder χ-axis; detector, Rigaku curved position sensitive proportional counter system; measuring range, 3–160° (2θ); and counting duration, 60 min. The obtained data were analyzed by Jade software (Materials Data Institute, USA).

Regions on the gypsum pellets having approximately the same size were analyzed using a micro-Fourier transform infrared absorption spectrometer (FT-530, Horiba, Tokyo) under the following conditions: measurement mode, reflection; measurement area, 20×40 μm; detector, ×16 mercury cadmium telluride cooled by liquid N_2; measurement range, 750–4000 cm^{-1}; resolution, 2 cm^{-1}; and scan cycle, 30.

Results

The thermal properties of the gypsum were checked by TG–DTA and DSC. The results obtained under several conditions were in accordance with the well-known thermal properties of gypsum, i.e., the thermal reactions were affected by the experimental conditions such as the heating rate, the sample weight and the atmosphere. Figure 1a shows a DSC curve of the gypsum clearly resolving the two endothermic reactions; the first endotherm at 397 K (124°C) corresponds to the transformation of gypsum $CaSO_4{\cdot}2H_2O$ to the hemi-hydrate form, bassanite $CaSO_4{\cdot}1/2H_2O$, and the second endotherm at 420 K (147°C) corresponds to the transformation from the hemi-hydrate to the dehydrate form, anhydrite $CaSO_4$. Figure 1b shows the TG and DTG curves of the gypsum. The weight loss accompanying the first dehydration was 15.27 wt%, and the second weight loss was 5.21 wt%; these values were compatible with the ideal water losses of three fourths for the first dehydration and one fourth for the second. These thermal reactions are reversible but slow, making it possible for us to trace the thermal history of gypsum irradiated by lasers.

Figure 2 shows an example of 3.0-μm LEBRA-FEL irradiation on a tooth sample. The pits formed by the irradiation obviously correlated with the power used. On lasing, a luminescence and a wisp of smoke were observed. Depth of pit was about 200 μm when the power of 5 mJ was applied and about 10 μm when 1 mJ was applied. Figure 3 shows an example of the effect of LEBRA-FEL

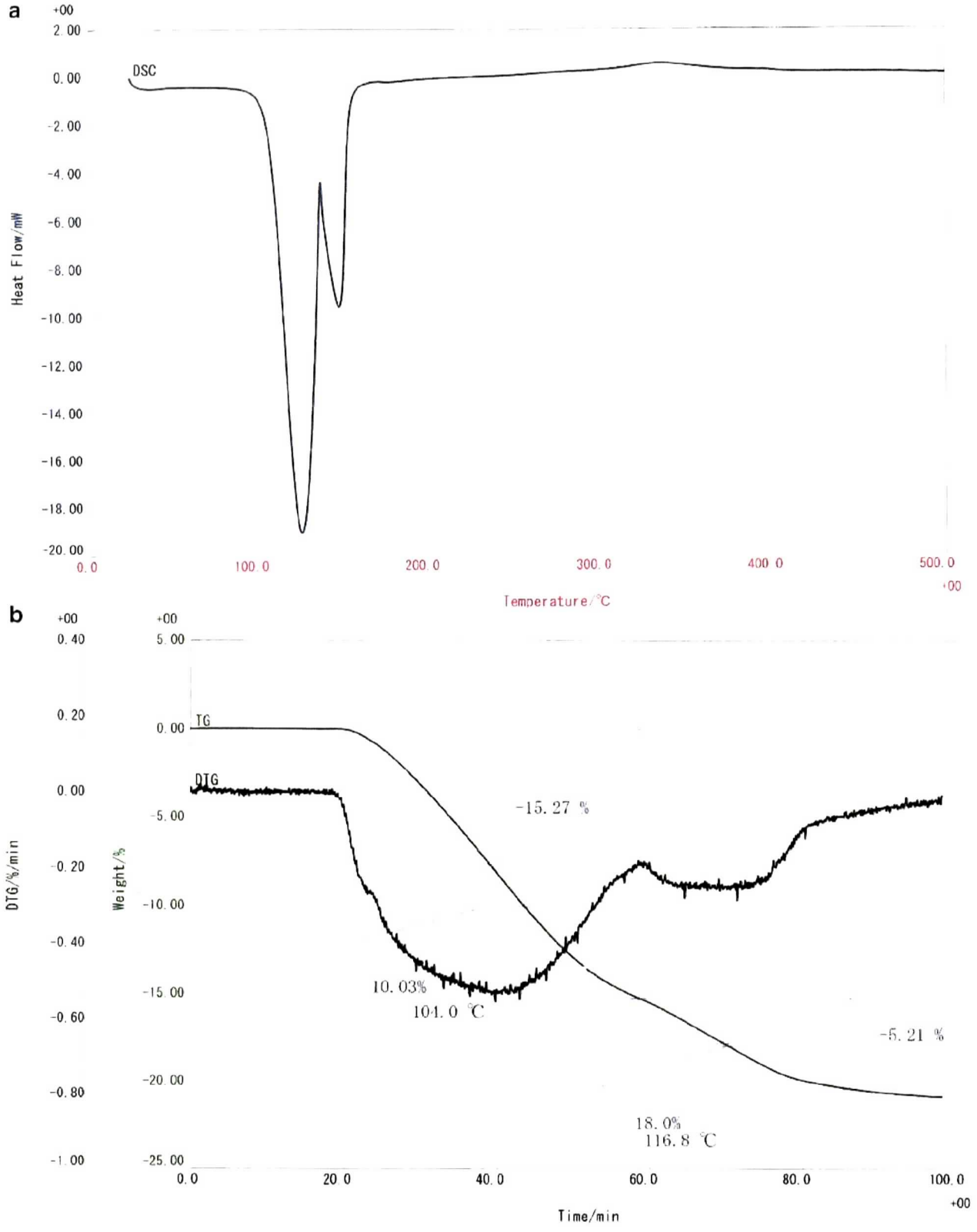

Fig. 1 **a** DSC curve (*top*) and **b** TG and DTG curves (*bottom*) of the gypsum. Two endothermic reactions at 124 and 147°C in **a** corresponded with the two weight loss reactions in **b**

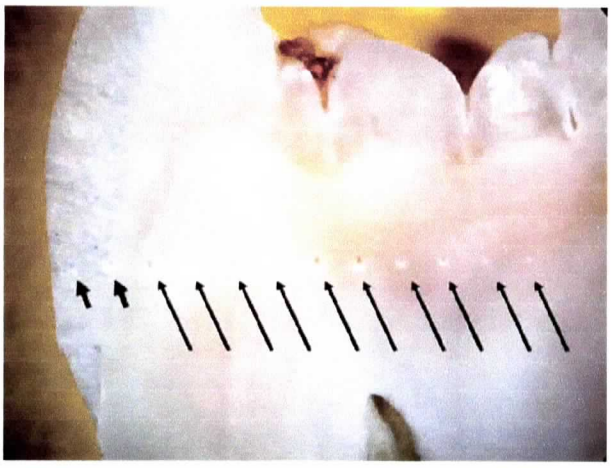

Fig. 2 Photograph of a 3.0-μm LEBRA-FEL irradiated human tooth section. Two points on the enamel surface (*short arrows*) were the results of repeated irradiation by the energy of 5 mJ, and ten points on the dentin surface were of repeated irradiation by varying the energy from 5 to 1 mJ at 1-mJ intervals from left to right (*long arrows*). Pits at the upper position were preliminary irradiation

irradiation on a gypsum pellet. After irradiation at a wavelength of 3.0 μm and a pulse energy of 2 mJ, pits having a diameter of about 150 μm were formed. In the irradiation on gypsum experiment, repeat number of laser irradiation was varied from one to three times. Depth of pit was in good correlation with the shot number. The size of pit was slightly but apparently greater in gypsum pellet than in human tooth section under the same conditions.

As Figs. 2 and 3 show, the depth of the pits depended on the power of irradiation. It was not possible to detect any trace of scorch marks in any of the irradiated gypsum pellets and human tooth sections using a binocular microscope. The pit size and depth quickly subsided when an irradiation wavelength other than 3.0 μm was used. No pit formation was observed after irradiation at wavelengths of 2.6 or 3.8 μm even at pulse energies as high as 20 mJ.

The micro-XRD measurements were carried out to identify crystalline materials in and around the pits formed by the LEBRA-FEL irradiation. They did not reveal any change in the crystalline structure (Fig. 4). The diffraction peaks observed were identified as those of gypsum (JSPS powder diffraction file number 33-0311). The peak intensities differed from those of the standard due to the orientation effect. Dehydrated forms of gypsum such as bassanite and anhydrite were not observed by micro-XRD although an 18-kW power source was used.

The micro-FTIR results also showed no evidence of change in the gypsum crystalline structure (Fig. 5). There were two absorption bands related to OH bending at about 1,600 cm^{-1} and two strong absorption bands related to OH stretching at around 3,400 and 3,550 cm^{-1}. These bands were observed in and around the pits formed by irradiation indicating that the water molecules in the gypsum were not released.

Discussion

In this study, to investigate the thermal effect on an irradiated sample, gypsum was selected as a thermally sensitive material, and micro-XRD and micro-FTIR were used to reveal whether thermal modification had occurred in gypsum. The thermal properties of gypsum are well known, and the phase transformations from gypsum to hemi-hydrate form, hemihydrate or mineral bassanite, and from bassanite to dehydrate form, anhydrite, are well established and also known that these transforming temperatures are influenced by the experimental conditions as well as the materials' purity [29–32]. The results of differential thermal analysis showed that the first transformation from gypsum to bassanite occurred at about 124°C and the second transformation from bassanite to anhydrite at about 147°C. Therefore, the presence of these materials in the irradiated gypsum pellets should be an exact evidence of the temperature history.

Using XRD, it is generally possible to detect the mixed crystalline forms as low as 1 wt%. Hirota and Furumoto [13] detected calcium pyrophosphate by micro-XRD at 10 kW in dental enamel that had been irradiated by a Er:YAG laser. Sakae et al. [26] found that the 3.0-μm LEBRA-FEL irradiation did not cause scorches on the human tooth samples, whereas, the 2.94-μm Er:YAG laser irradiation did. In this study, no other phase besides the original gypsum was detected by micro-XRD, although an 18-kW power source was used, indicating that the remaining pit walls were intact. Therefore, the rise of temperature caused by LEBRA-FEL irradiation was less than 124°C. These

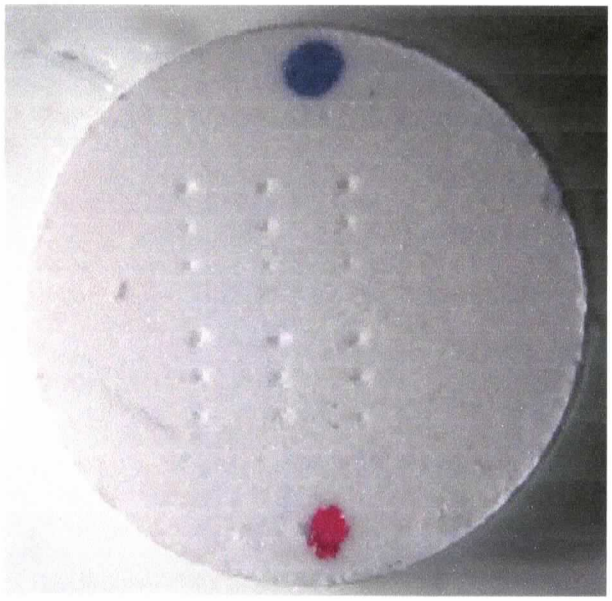

Fig. 3 Photograph of the 3.0-μm LEBRA-FEL irradiated gypsum pellet. Three pits at *top left* were the results of three, two and one irradiation shot from top to bottom. The same experiment was repeated six times on this gypsum pellet

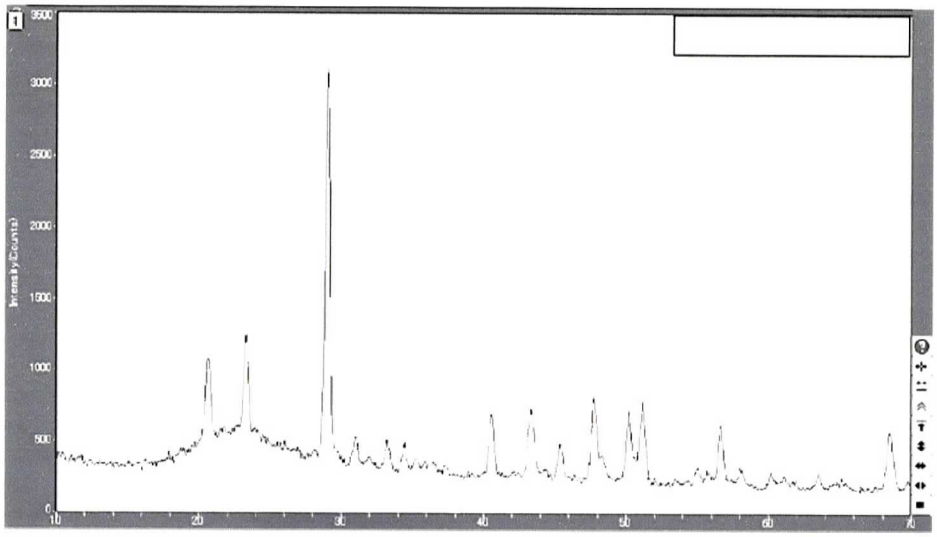

Fig. 4 Micro-XRD pattern of the gypsum. Abscissa is the diffraction angle, 2θ (CuKα), and ordinate is the diffraction intensity

findings and the observation of luminescence and smoke on the irradiation suggested that the ablation mechanism of LEBRA-FEL irradiation is mainly plasma or evaporative ablation rather than thermal ablation.

In this study, the irradiation power and wavelength were varied to examine the ablation effect. However, other factors such as pulse duration or pulse interval were not varied. Compared with the reported Er:YAG laser irradiation results, ultra short-pulsed laser [33–35] and Q-switched lasers were effectively deducing the thermal effects [36]. The LEBRA-FEL has a 20-μs macro-pulse at 2 Hz with less than 1 ps micro-pulses at 350-ps interval [27, 28]. The LEBRA-FEL has an effect on the pit formation using the power as low as 2 mJ/pulse in contrast to several 100-mJ power used in dental clinical Er:YAG instrument. Er:YAG caused thermal effects on dental hard tissues [37]. The LEBRA-FEL study was compared with the results of the FEL at Vanderbilt University where no thermal cracking can be observed after ablation in dentin; however, a small amount of thermal cracking can be observed after ablation in enamel [16]. The small but appreciable difference in the irradiated dentins might be due to the FEL micro-pulse structures.

Other factors that may affect ablation include the structure and texture of the material. The cause of inconsistency of the effective wavelength range between gypsum and dental hard tissues remained to be clarified, from 2.6 to 3.8 μm for the former and from 2.0 to 4.0 μm for the latter. In our preliminary laser irradiation investigation using natural and synthetic hydroxyapatite, the degree of crystallinity and grain size influenced the results (unpublished data). To clarify the laser irradiation effects on biological hard tissues that are composed of biological apatites, all these factors should be controlled in addition to taking into account the chemical inhomogenity of the hard tissues [38].

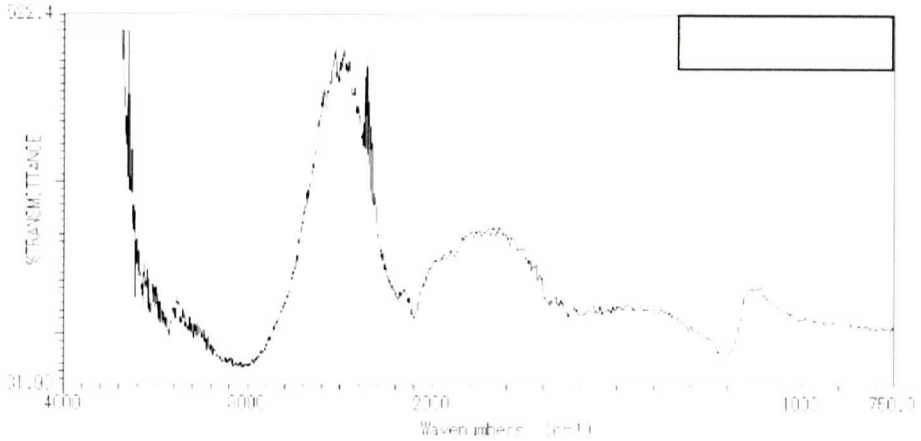

Fig. 5 Micro-FTIR spectra of the gypsum (K-K transformed). Faint but appreciable bands at 3,400 and 3,550 cm^{-1} were due to OH stretching modes of gypsum

Acknowledgements The authors would like to thank all the members at LEBRA, Nihon University for their operation and management of LEBRA-LINAC and LEBRA-FEL. This study was supported by a Grant-in-Aid for Scientific Research (no. 17591927) from the Japan Society for the Promotion of Science, Japan, and the Frontier Science Projects to LEBRA, 2000 and 2005 from the Ministry of Education, Culture, Sports, Science and Technology, Japan.

References

1. van As G (2004) Erbium lasers in dentistry. Dent Clin North Am 48:1017–1058
2. Lobene RR, Bhussry BR, Fine S (1968) Interaction of carbon dioxide laser radiation with enamel and dentin. J Dent Res 47:311–317
3. Kantola S, Laine E, Tarna T (1973) Laser-induced effects on tooth structure. VI. X-ray diffraction study of dental enamel exposed to a CO_2 laser. Acta Odontol Scand 31:369–379
4. Goodman BD, Kaufman HW (1977) Effects of an argon laser on the crystalline properties and rate of dissolution in acid of tooth enamel in the presence of sodium fluoride. J Dent Res 56:1201–1207
5. Kuroda S, Fowler BO (1984) Compositional, structural, and phase changes in in vitro laser-irradiated human tooth enamel. Calcif Tissue Int 36:361–369
6. Fowler BO, Kuroda S (1986) Changes in heated and in laser-irradiated human tooth enamel and their probable effects on solubility. Calcif Tissue Int 38:197–208
7. Nelson DGA, Wefel JS, Jongebloed WL, Featherstone JDB (1987) Morphology, histology and crystallography of human dental enamel treated with pulsed low-energy infrared laser radiation. Caries Res 21:411–426
8. Bachmann L, Craievich AF, Zezell DM (2004) Crystalline structure of dental enamel after Ho:YLF laser irradiation. Arch Oral Biol 49:923–929
9. Feuerstein O, Mayer I, Deutsch D (2005) Physico-chemical changes of human enamel irradiated with ArF excimer laser. Lasers Surg Med 37:245–251
10. LeGeros RZ, Bonel G, Legros R (1978) Types of "H2O" in human enamel and in precipitated apatites. Calcif Tissue Res 26:111–118
11. Palamara J, Pharkey PP, Rachinger WA, Orams HJ (1987) The ultrastructure of human dental enamel heated in the temperature range 200°C to 600°C. J Dent Res 66:1742–1747
12. Sakae T (1988) X-ray diffraction and thermal studies of crystals from the outer and inner layers of human dental enamel. Arch Oral Biol 33:707–713
13. Hirota F, Furumoto K (2003) Temperature rise caused by laser (CO_2, Nd:YAG, Er:YAG) irradiation of teeth. Int Congr Ser 1248:301–304
14. Sonntag KD, Klitzman B, Burkes EJ, Hoke J, Moshonov J (1996) Pulpal response to cavity preparation with the Er:YAG and mark III free electron lasers. Oral Surg Oral Med Oral Pathol Oral Radiol Endo 81:695–702
15. Ogino S (1996) The FEL surface modification of tooth dentin. Zairyo 45:1254–1255
16. Ostertag M, Walker R, Weber H, van der Meer L, McKinley J, Tolk N, Jean B (1996) Ablation in teeth with the free-electron laser around the absorption peak of hydroxyapatite (9.5 μm) and between 6.0 and 7.5 μm. Proc SPIE Int Soc Opt Eng 2672 (Lasers in Dentistry II):181–192
17. Ogino S, Awazu K (1997) Free electron laser (FEL) induced desorption of ions from tooth dentin. Proc SPIE 2973:29–38
18. Ogino S, Awazu K (1998) Surface treatment of dentin by FEL ablation. Mol Electr Bioelectr 9:51–55
19. Ogino S, Awazu K (1998) The surface modification of tooth dentin with a free electron laser (FEL). Nucl Instrum Methods Phys Res B 144:236–239
20. Liu NQ, Li YG, Zhu JB, Zhang LW, Wang MK, Wu G, Yang XP, Li GC, Huang YY, Dong YM, Gao XJ (2001) Compositional change in humane enamel irradiated with MIR free electron laser. Chin Sci Bull 46:2016–2018
21. Swift EJ Jr, Edward GS, Perdigao J, Thompson JY, Nunes MF, Ruddell DE, Negishi A (2001) Free-electron laser etching of dental enamel. J Dent 29:347–353
22. Junbiao Z, Yonggui L, Nianqing L, Guoqing Z, Minkai W, Gan W, Xuepin Y, Yuying H, Wei H, Yanmei D, Xuejun G (2001) Primary experimental studies on mid-infrared FEL irradiation on dental substances at BFEL. Nucl Instrum Methods Phys Res A475:630–634
23. Iida H, Kimura M, Yamamoto N, Hirayama S, Ikemi T, Irokawa K, Kuroda H (2002) A study of tooth structure irradiated with IR-FEL. Jpn J Appl Phys Part 1, 41(Suppl):148–151
24. Heya M, Awazu K (2002) Wavelength and average power density dependency of the recrystallization of root dentin using an MIR-FEL. Proc SPIE 4633:201–209
25. Heya M, Sano S, Takagi N, Fukami Y, Awazu K (2003) Wavelength and average power density dependency of the surface modification of root dentin using an MIR-FEL. Lasers Surg Med 32:349–358
26. Sakae T, Sato Y, Tanimoto Y, Higa M, Oinuma H, Kozawa Y, Okada H, Yamamoto H, Hayakawa T, Nemoto K, Sakai T, Nogami K, Mori A, Kuwada T, Hayakawa Y, Tanaka T, Hayakawa K, Sato I (2005) Pit formation in human enamel and dentin irradiated using the 2.94 mm LEBRA-free electron laser. Int J Oral Med Sci 4:8–13
27. Hayakawa Y, Sato I, Hayakawa K, Tanaka T, Nakazawa H, Yokoyama K, Kanno K, Sakai T, Ishiwata K, Enomoto A, Fukuda S, Ohsawa S, Tsuchiya K, Kato (2002) First lasing of LEBRA FEL at Nihon University at a wavelength of 1.5 μm. Nucl Instrum Methods Phys Res A 483:29–33
28. Tanaka T, Hayakawa K, Hayakawa Y, Mori A, Nogami K, Sato I, Yokoyama K, Ishiwata K, Kanno K, Nakao K, Sakai T (2004) Tunability and power characteristics of the LEBRA infrared FEL. Proceedings of the 2004 FEL Conference, p 247–250
29. Murakami K, Shimamura Y, Tanaka H (1957) Dehydration temperature of gypsum. Sekko to Sekkai 1:1522–1528
30. Fleck WEP, Jones MH, Kuntze RA, McAdie HG (1960) Differential thermal analysis of natural and synthetic hydrates of calcium sulfate. Can J Chem 38:936–943
31. Marcoen JM (1974) Application of differential thermal analysis, infrared spectrometry, and X-ray diffraction to the study of different crystalline states of a hydrated mineral, gypsum. Bull Rech Agron Gembloux 9:13–27
32. Sarma LP, Prasad PSR, Ravikumar N (1998) Raman spectroscopic study of phase transitions in natural gypsum. J Raman Spectrosc 29:851–856
33. Strassl M, Wieger V, Wintner E (2005) Novel approach for dental hard tissue ablation by ultra-short laser pulses. Trends Optics Photonics 98(Advanced Solid-State Photonics):819–825
34. Kohns P, Zhou P, Stormann R (1997) Effective laser ablation of enamel and dentine without thermal side effects. J Laser Appl 9:171–174
35. Lizarelli RF, Kurachi C, Misoguti L, Bagnato VS (2000) A comparative study of nanosecond and picosecond laser ablation in enamel: morphological aspects. J Clin Laser Med Surg 18:151–157
36. Kermani O, Lubatschowski H, Asshauer T, Ertmer W, Lukin A, Ermakov B, Krieglstein GK (1993) Q-switched CTE:YAG (2.69 microns) laser ablation: basic investigations on soft (corneal) and hard (dental) tissues. Lasers Surg Med 13:537–542
37. Dostalova T, Jelinkova H, Krejsa O, Hamal H (1996) Evaluation of the surface changes in enamel and dentin due to possibility of thermal overheating induced by Erbium:YAG laser radiation. Scanning Microsc 10:285–290
38. LeGeros RZ, Sakae T, Bautista C, Retino M, LeGeros JP (1996) Magnesium and carbonate in enamel and synthetic apatites. Adv Dent Res 10:225–231

Journal of Mineralogical and Petrological Sciences, Volume 101, page 10-13, 2006

Application of LEBRA-PXR to the diffraction analysis of minerals

Toshiro SAKAE*, Yasushi HAYAKAWA**, Akira MORI**, Takao KUWADA**, Takeshi SAKAI**, Kyoko NOGAMI**, Toshinari TANAKA**, Ken HAYAKAWA** and Isamu SATO**

*Department of Histology, Embryology and Anatomy, Nihon University School of Dentistry at Matsudo, Chiba 271-8587, Japan
**LEBRA, Laboratory for Electron Beam Research and Application, Institute of Quantum Science, Nihon University, Narashino-dai, Funabashi 274-8501, Japan

Parametric X-rays (PXR) are a new type of X-ray that are generated by crystal-electron interactions. The Laboratory for Electron Beam Research and Application (LEBRA) at Nihon University generates PXR using a double-crystal system generating electrons from a 100-MeV class LINAC. LEBRA-PXR has potential for use as a wavelength tunable, ultra-high bright X-ray source with a macro-/micro-pulse structure. LEBRA-PXR has an energy-dispersion in the horizontal axis, assumed to be 0.2% in the experimental window, but can be used as monochromatic X-ray source for diffraction using a simple slit-system. A diffraction experiment was successfully carried out by applying an 11 keV, or 1.1273 Å, LEBRA-PXR. Near-perfect crystals, such as graphite used for a monochromator showed sharp diffraction peaks. Clear, transparent mineral quartz and fluorapatite crystals also showed sharp diffraction peaks, while the diffraction peaks from clear calcite and silicon powder were not detected. Possible reasons for the lack of diffraction peaks from these materials are discussed. LEBRA-PXR has potential for use in studies on the diffraction of other materials, and is therefore, expected to be a useful tool for crystallographic analysis.

Keywords: Parametric X-ray, Diffraction, Graphite, Quartz, Calcite, Apatite

INTRODUCTION

Parametric X-rays (PXR) are radiation emitted by charged particles moving in a crystal. They were first observed experimentally by Vorobiev et al. (1985) and Didenko et al. (1985) in 1985 at Tomsk in the Soviet Union, who identified the radiation from relativistic electrons in a crystal in the Bragg direction. Since then, the term, "parametric X-ray radiation", or PXR, has been used in investigations into this phenomenon. Schagin (2001) and Krasilnikov et al. (2005) have reviewed the theoretical and experimental approaches on PXR.

Linear electron accelerators, LINACs, are usually used to generate PXR, as they can provide short, high-current, electron beam pulses. Such electron beams can generate short PXR pulses at powers of about a megawatt per steradian. Numerous experimental studies have shown that PXR exhibits sharp maxima in the vicinity of the Bragg direction relative to the crystallographic plane, and that PXR reflections have a conical shape with an angular size of about or greater than the inverse relativistic factor of the incident particles (Schagin, 2001).

PXR has a macro/micro-pulse structure that depends on the macro/micro-pulse structure of the electron beam generated in the LINAC system, which usually generates pico- or nano-second micropulses. It is hoped that PXR can act as a new short-pulse brilliant X-ray source for a wide variety of applications, from basic research to medical applications. The Laboratory for Electron Beam Research and Application (LEBRA) at Nihon University in Japan, generates PXR via a double-crystal system using electrons from a 100 MeV class LINAC (Hayakawa et al., 2005), and has recently successfully applied LEBRA-PXR to the diffraction analysis of minerals. This paper discusses the results of our study into the PXR diffraction of these selected crystals.

GENERATION OF LEBRA-PXR

The LINAC at LEBRA is a conventional system that is not equipped with any special devices, such as an RF gun or a sub-harmonic buncher. The LEBRA-LINAC specifications are listed in Table 1. Since the LEBRA-LINAC has been developed as a free electron laser (FEL) source,

T. Sakae, sakae.toshiro@nihon-u.ac.jp Corresponding author

Table 1. Specification of LEBRA-LINAC

Beam energy	50 – 125 MeV
Acceleration frequency	2856 MHz
DC gun voltage	-100 kV
Macro pulse	2 Hz
Beam pulse duration	20 μs
Micro pulse	350 ps
Bunch length	2 - 3 ps
Beam current	200 mA
Repetition rate	12.5 Hz
Average current	50 μA
Normalized emittance (rms)	<20π mm mrad

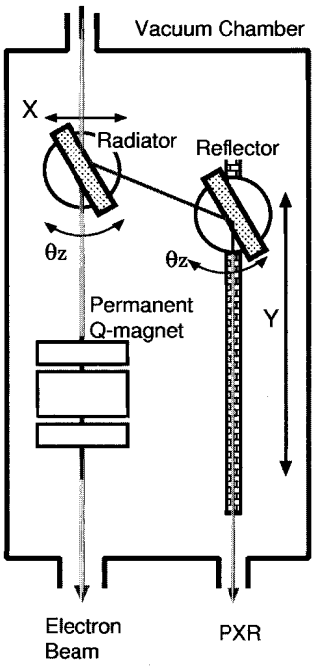

Figure 1. LEBRA-PXR double-crystal system.

high-current electron beams with a low emittance are obtained. To meet the demand for high brilliant wavelength-tunable monochromatized X-rays suitable for a wide range of applications from basic research to medical diagnosis, a double-crystal system was constructed at LEBRA to generate the PXR (Fig. 1). Details of the construction of the LEBRA-PXR system are described in Hayakawa et al. (2005). In our study, the LEBRA-PXR was operated at 11.00 keV, or 1.1273 Å. At present, the LEBRA-PXR has an energy-dispersion along the horizontal axis, which is assumed to be 2% in the experimental full-window width of 13 cm, and 0.2% in the diffraction window width of 1 cm. With a limiting millimeter-sized slit, the LEBRA-PXR can be used as monochromatic X-ray source for diffraction experiments.

DIFFRACTION ANALYSIS

Diffraction Recording

Powder diffraction data from the materials of interest was collected using a normal goniometer (Rigaku, Japan). This system did not have the usual slit or monochromatic systems, because the LEBRA-PXR itself generated highly monochromatized X-rays. The divergence of the LEBRA-PXR was limited by placing X-ray absorbable bricks before the sample to obtain a 1 cm irradiation width at the sample position. The diffraction data was counted using a 35 mm diameter, 60 mm long ion chamber, using an accelerating voltage of 1 kV, an argon gas purge, and a position fixed at the 2θ diffraction angle. An ion camber was selected as the counting device, because the PXR laboratory is in a high energy-field, and noise is generated by the LINAC. The material of interest was placed in the sample holder, and the measurement was carried out in the θ-scan mode. The goniometer system used was not fully adopted in the auto-scan measurements, and the counts were manually recorded at 0.001-degree intervals.

Materials

The materials selected for studies on PXR diffraction were: (i) a graphite crystal used in an X-ray diffraction monochromator, (ii) a large, clear transparent quartz crystal, about 3 cm in length obtained from Brazil, (iii) a large, clear faint greenish transparent fluorapatite crystal, about 2 cm in length obtained from Durango, Mexico, and (iv) a clear transparent calcite crystal, about 2 cm in length obtained from China, which exhibited internal cleavages. These crystals were mounted in plastic frames, and plastic clay was used to fix the crystal in the goniometer sample holder to orientate the crystal surface to the PXR beam. Conventional X-ray diffraction patterns of the samples were recorded using an X-ray diffractometer (XRD, Rigaku Model RINT-2500, Japan) for comparison with the LEBRA-PXR diffraction patterns. Peak identification and FWHM calculations were carried out using the JADE software package (Materials Data Inc., USA).

RESULTS

The conventional X-ray diffraction patterns obtained for graphite, calcite, and fluorapatite are shown in Figure 2. Any diffraction peaks from quartz that overlap the graphite peaks are excluded for clarity. These diffraction patterns, including those of quartz, fitted database data well: PDF No. 26-1079 for graphite, PDF No. 46-1045 for

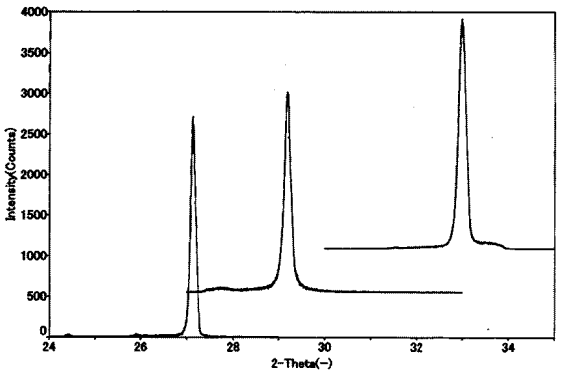

Figure 2. The conventional X-ray diffraction patterns for the Graphite (Left), Calcite (Middle), and Fluorapatite (Right) mineral crystals. The vertical axis was scaled arbitrary and shifted for ease to see.

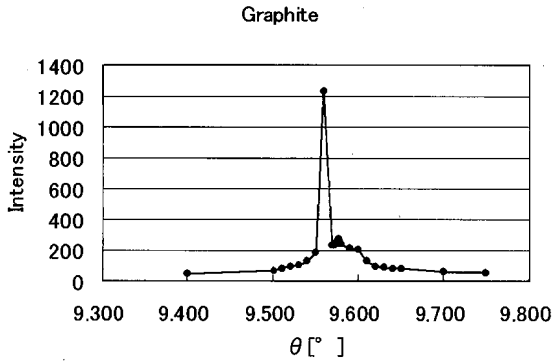

Figure 3. LEBRA-PXR diffraction of "Graphite" crystal.

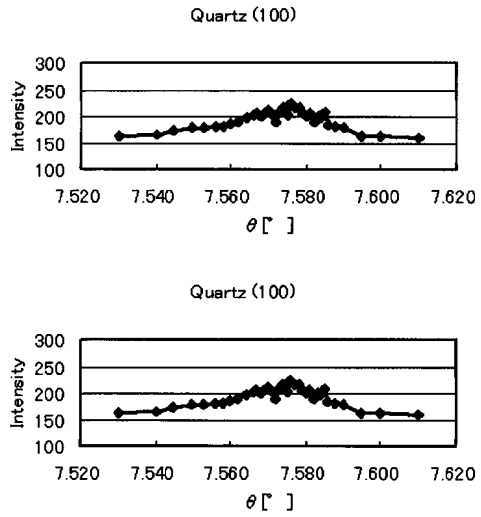

Figure 4. LEBRA-PXR diffraction from "Quartz ". Top: 100 reflection, and bottom: 200 reflection.

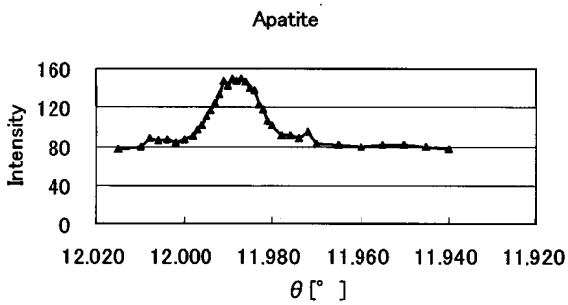

Figure 5. LEBRA-PXR diffraction from "Fluorapatite".

quartz, PDF No. 47-1743 for calcite, and PDF No. 15-0876 for fluorapatite. The FWHM values of the samples were: $FWHM_{003} = 0.117°$ for graphite, $FWHM_{101} = 0.168°$ for quartz, $FWHM_{104} = 0.173°$ for calcite, and $FWHM_{211} = 0.189°$ for fluorapatite.

The observed LEBRA-PXR diffraction peaks in the θ-scan mode for graphite, quartz, and fluorapatite are shown in Figures 3, 4 and 5. Each of these diffraction patterns was confirmed by reverse scanning. Table 2 lists the diffraction data of these materials. The LEBRA-PXR diffraction data of graphite was the most clear of the materials tested. The 100 and 200 reflections of quartz clearly show that neither noise nor any other artifact caused these

Table 2. LEBRA-PXR Diffraction data for the "Graphite", "Quartz", "Fluorapatite", and "Calcite" crystals

	Graphite	Quartz	Quartz	Fluorapatite	Calcite
Diffraction					
hkl	0 0 2	1 0 0	2 0 0	3 1 1	1 0 4
d-value	3.3756	4.2550	2.1277	2.1400	3.035
$2\theta_{calc}$	19.22	15.22	30.12	30.54	21.41
θ_{calc}	9.61	7.61	15.06	15.27	10.71
Maximum θ_{obs}	9.55	7.575	15.3	15.3	n.d.
Intensity	1150	70	60	70	n.d.
Expected Intensity based on Graphite	1150	80	30	13	296
JCPDS card #	41-1487	46-1045		15-0876	05-0586
I/Io(RIR)	7.78	3.41	6.0	1.5	2.0
I *hkl* /Io	100.0	16.0		6.0	100.0

LEBRA-PXR wavelength was 1.1273 Å (11.00 KeV)

maxima. However, the 200 diffraction peak of quartz was irregular in shape.

DISCUSSION

We successfully carried out diffraction experiments using LEBRA-PXR. A number of reports pertaining to PXR have been published after the original work of Didenko et al. (1985) and Vorobiev et al. (1985), but almost all of these have been concerned with production techniques and the theory of PXR. There were no reports on the application of PXR to diffraction among the 32 reports found on PXR found using a CrossSearch program (ISI) using the search items, "parametric" and "X-ray". In this context therefore, our study is the first report of the application of PXR to diffraction.

In a preliminary study, we found empirically that LEBRA-PXR diffraction was very sensitive to the homogeneity of a crystal. Trials using large, flat mica crystals did not show any reflections. Mica was used by Bragg (1912) in the first X-ray diffraction experiments that led him to develop his theory of "Bragg reflections" (Bragg, 1913). This may be due to the layered structure of the mica having macroscopic imperfections in the crystal planes, but also could be due to the flexibility of the mica crystals that could lead to out-of-plane misalignments. Using the crystal surface of natural mineral crystals, the diffraction peaks of quartz and fluorapatite could be obtained. It was notable that in our experiments, no diffraction data for calcite was obtained. The reason for this is unclear, but we assume that there may be several causes. Even though calcite was clear and transparent at the macroscopic level, there could be cleavages at the atomic scale in the crystal, giving the calcite mosaic-like features at the microscopic level. Another possibility for the lack of diffraction data for calcite may be attributed to the ultra-high crystallinity of the materials used in our experiments. In such a case, the diffraction peaks may too sharp to be detected using a $2\theta = 0.001°$ measurement interval. However, the X-ray diffraction peaks of the materials taken using the conventional XRD powder diffractometer were not so highly ordered and crystalline, as shown in Figure 2. Another reason why no calcite diffraction peaks were detected was that the calcite diffraction spots were outside the narrow range of the detector. This can be easily understood in the case of X-ray diffraction data collection from a single crystal. This may be also the reason why the 002 reflection of quartz was distorted, as shown in Figure 4.

In trials using standard silicon powder diffraction material, we failed to observe any diffraction data. This seems to suggest that LEBRA-PXR requires a macroscopically large and perfect crystal for diffraction analysis. We are presently developing a powder diffraction system using LEBRA-PXR. The diffraction peak intensities obtained from LEBRA-PXR were very weak, as shown in Table 2. This may be partly due to the ultra short pulses from the LEBRA-PXR: the 20 ms 2-Hz duration of the macro pulse the electron bunch length became a 2-350 ps micro-pulse cycle. This means the net duration of the radiation pulse was only about 0.2 ms per 1 sec LEBRA pulse. In other words, LEBRA-PXR is a high brilliance short-pulse X-ray source. This study has shown that LEBRA-PXR is a useful tool for diffraction analysis.

ACKNOWLEDGMENTS

This study was carried out at LEBRA, Nihon University, Japan, with the help of many staff and assistants. The authors wish to thank all our colleagues at LEBRA. This study was supported by the Academic Frontier Project at LEBRA, Nihon University, Japan, and a Grant-in-Aid for Scientific Research from Nihon University (Sogo:04-019, TS).

REFERENCES

Bragg, W.L. (1912) The specular reflection of X-rays. Nature, 90, 410.

Bragg, W.L. (1913) The structure of some crystals as indicated by their diffraction of X-rays. Proceedings of the Royal Society, A, 89, 248-260.

Didenko, A.N., Kalinin, B.N., Pak, S., Potylitsin, A.P., Vorobiev, S.A., Baryshevsky, V.G., Danilov, V.A. and Feranchuck, I.D. (1985) Observation of monochromatic X-ray radiation from 900 MeV electrons transmitting through a diamond crystal. Physics Letters A 110, 177-179.

Hayakawa, Y., Sato, I., Hayakawa, K. and Tanaka, T. (2005) Simulations to the project of a PXR based X-ray source composed of an electron linac and a double-crystal system. Nuclear Instruments and Methods in Physics Research Section B: Beam Interactions with Materials and Atoms, 227, 32-40.

Krasilnikov, V. Nasonov, N. and Zhukova P. (2005) Relative contribution of real and virtual photon diffraction to the parametric X-ray yield. Nuclear Instruments and Methods in Physics Research, B277, 55-62.

Shchagin, A.V. (2001) Current status of parametric X-ray radiation research. Radiation Physics and Chemistry, 61, 283-291.

Vorobiev, S.A., Kalinin, B.N., Pak, S. and Potylitsin, A.P. (1985) Discovery of monochromatic X-rays at interaction of ultrarelativistic electrons with diamond crystal. Pis'ma v Zhurnal Eksperimental'noi i Teoreticheskoi Fiziki, 41, 3-6.

Manuscript received February 28, 2005
Manuscript accepted August 26, 2005
Manuscript handled by Eiji Ohtani

AB 2006

QUANTITATIVE RADIOGRAPHIC STUDY OF NEW BONE FORMED AROUND THE IMPLANT USING A NEWLY DEVELOPED PARAMETRIC X-RAY METHOD

T. Sakae[1*], T. Suwa[2], Y. Numata[2], H. Nakada[2], I. Sato[3], and R. Z. LeGeros[4]

[1] Department of Histology, Cytology, and Anatomy, and
[2] Department of Development, Gnatho-Oral Prostetic Rehabilitation,
Nihon University School of Dentistry at Matsudo, 271-8587, Japan,
[3] Laboratory for Electron Beam Research and Application, Nihon University, 271-8501, Japan,
[4] Department of Biomaterials and Biomimetics, New York University College of Dentistry, NY, NY 10010, USA

[*] sakae.toshiro@nihon-u.ac.jp

Abstract: **New bone formed around the implant was classified into three categories by Nakada et al and Suwa et al. The purpose of this study was to determine structural and radiographic characteristics of these bones using a newly developed wavelength tunable and highly parallel Parametric X-ray (PXR) method. Methods: PXR was generated by a LINAC at LEBRA, Nihon University. X-ray wavelength was tuned from 7 KeV, 0.177 nm, to 16 KeV, 0.0775 nm. Ti6Al4V alloy implants with surfaces modified by coating or grit-blasting were implanted into rabbit tibia bones for 2, 4, and 8 weeks. After sacrifice, implant with surrounding bones was isolated and non-demineralized polished thin sections were prepared. PXR conditions; PXR macro pulse: 20 micro-sec; micro-pulse: 2-3 pico-sec with 350 pico-sec duration; irradiation: 900 sec; sample-detector distance: 7.5 mm; films: Fuji Film Imaging Plate. The images obtained were processed using an image analyzer. Results: PXR radiography showed distinct difference between the newly formed bone and the compact bone. Color-mapping of the images showed the changes in bone formation with time of implantation. Conclusion: LEBRA-PXR is a good tool for the quantitative analysis of bone formation.**

Introduction

Osseointegration of implants has been the subject of many investigations. Nakada et al. [1, 2] classified the newly formed bone around and/or attached to Ti alloy implanted in rabbit tibia bone into three categories: (a) closely attached to the compact bone, (b) surrounding the implant, and (c) occurring at the bone marrow spaces or medullary cavities. These authors carefully investigated these bones using polarized light microscopy and Roentgen micro-radiography. Suwa et al. [3] showed crystallographic differences in the newly formed bones.

The aim of this study was to determine structural and histological differences of these bones using a newly developed wavelength tuneable Parametric X-ray, PXR.

Materials and Methods

Animal experiment: New Zealand White rabbits, thirteen week old, were used in this study. Titanium alloy (Ti6Al4V), 2.8 mm in diameter and 8.0 mm in length and grit-blasted with alumina powder abrasive, were implanted in the tibia bone (Fig. 1). The Nihon University School of Dentistry at Matsudo Experimental Animal Ethics Committee (ECS-03-0003) approved the experimental protocol for the use of the animal. After one-, two-, or four-week implantation the rabbits were sacrified under anesthesia. Non-demineralized polished sections, 50 μm in thickness, were prepared.

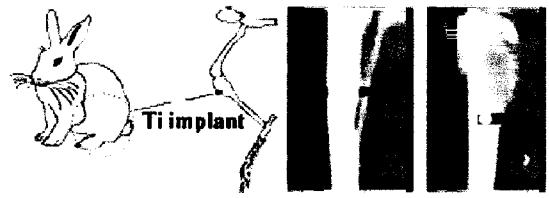

Fig. 1 (Left) Schematic representation of implantation of Ti alloy implant into the rabbit tibia bone. (Right) Roentgen images of the implanted bone [3].

Parametric X-ray experiment: Parametric X-ray, PXR, is an emergent X-ray which can be generated by irradiating electrons to a crystal. LEBRA, Laboratory for Electron Beam Research and Application, at Nihon University succeeded in generating PXR using a 100 MeV LINAC and applying it to several kinds of X-ray experiments (Fig. 2) [4-6]. PXR has many unique characteristics, the most important of which is tuneable highly coherent and highly monochromatized X-ray wavelength (nm), or X-ray energy (KeV). X-ray

attenuation of material varies depending on the wavelength, causing changes in radio-opacity. Particular materials of interest, for example bone tissues in this study, can be distinguished by selecting the X-ray wavelength. Imaging Plate, Fuji film Co., was used in this study for its wide dynamic range and fine linearity.

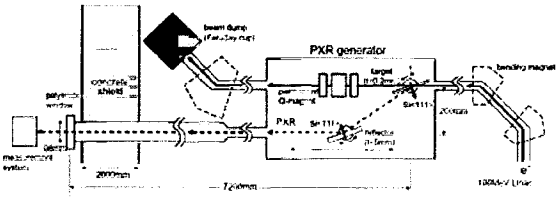

Fig. 2. Schematic representation of the generation of tuneable wavelength Parametric X-ray, PXR [5].

Results

Figure 3 shows the effects of PXR wavelength variation to the recorded images. Ti-implant interface image became more distinct with the increase in X-ray energy from 15 KeV (0.0827 nm) to 17 KeV (0.0730 nm). In general, the higher X-ray energy means higher potential of X-ray penetration through the material. Thus, using the 17 KeV PXR showed more radio-translucency than using the 15 KeV PXR.

Fig. 3. Wavelength dependent radio-opacity. Note that Ti-implant interface is more distinct and clearer with the increase in X-ray energy. (From left to right: 15 KeV, 16 KeV, 17 KeV)

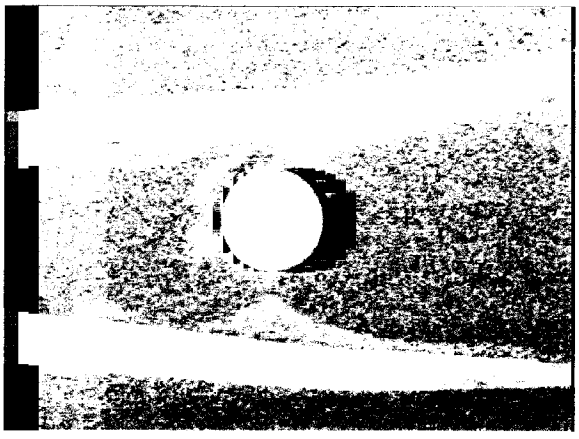

Fig. 4. PXR micro-radiogram of the Ti-implant imbedded rabbit tibia bone section. Difference in radio-opacity for the newly formed bone tissues was clearly shown.

Figure 4 shows a Roentgen image of the implanted bone using the PXR. In this figure the newly formed bones are clearly distinguishable: the attached bone, the surrounding bone, and the bone formed in the medullary cavity.

Figure 5 shows the result of a quantitative analysis of the recorded image. Following the quantitative calculation of the degree of calcification from the X-ray micro-radiogram [7, 8], the degree of radio-opacity was converted to estimated hydroxyapatite % content with the help of the aluminium step-wedge.

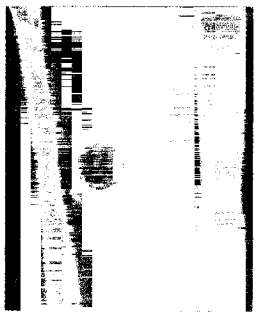

Fig. 5. Gray-scaled (originally pseudo-color) representation of Ti-implanted rabbit tibia bone. Aluminium step-wedge was located beside as for X-ray attenuation standard.

Discussion

LEBRA-PXR easily allows controlled changes of the highly monochromatized X-ray wavelength easily. As shown in Figure 3, radio-opacity of the material was dependent on the X-ray wavelength used. When using a standard dental Roentgen system, the fine structures shown in Figure 4 could not be distinguished [1]. The clear images obtained by PXR were due not only to the highly monochromatized but also highly-ordered parallel X-ray beam which did not cause obscure images.

The monochromatized X-ray has an advantage in quantitative analysis of the degree of calcification of bone. When using X-rays from usual generators which contain several characteristic X-rays or white X-ray, some special instrument such as graphite monochrometer, is required to obtain monochromatized X-ray [8]. Combination of the wavelength tuneablity and monochromatized character of PXR will provide a quick and precise quantitative radiographic analyser.

Conclusions

Application of LEBRA-PXR to radiographic analysis of rabbit bone resulted in good resolution of the images obtained. The high-power, highly monochromatized and highly parallel oriented X-ray resulted in an easy radiographic analysis including quantitative analysis.

Acknowledgements

The authors acknowledge the help of the members of LEBRA at Nihon University. This study was supported in part by the Grant-in-Aid for Scientific Research (No.17591927) from the JSPS, Japan, the

Grant-in-Aid for Scientific Research (S04-019, S05-029) from Nihon University, and the Frontier Science Projects to LEBRA at Nihon University, 2000 and 2005, from the MEXT, Japan.

References

[1] NAKADA, H., SAKAE, T., SUWA, T., LEGEROS, R.Z., GUNJI, A., KATO, T., KOZAWA, Y. AND KOBAYASHI, K. (2005): Observation of newly formed bone around implants using Parametric X-ray, *J.Hard Tissue Biol.*, **14**, pp. 1-4

[2] NAKADA, H., SAKAE, T., SUWA, T., LEGEROS, R.Z., KATO, T., AND KOBAYASHI, K. (2006): Observation of newly formed bone around dental implants using parametric x-ray, *Key Engineering Materials,* **309-311** (Pt.1, Bioceramics), pp. 31-36

[3] SUWA, T., SAKAE, T., NAKADA, H., LEGEROS, R.Z., AND KOBAYASHI, K. (2006): Variation in composition of bone surrounding implants, *Key Engineering Materials,* **309-311** (Pt.1, Bioceramics), pp. 19-22

[4] HAYAKAWA, Y., HAYAKAWA, K., INAGAKI, M., KUWADA, T., MORI, A., NAKAO, K., NOGAMI, K., SAKAE, T., SAKAI, T., AND SATO, I. (2006): Advanced applications of PXR at LEBRA, Nihon University, *Channelling,* (in press)

[5] HAYAKAWA Y., SATO, I., HAYAKAWA, K., TANAKA, T., MORI, A., KUWADA, T., SAKAI, T., NOGAMI, K., NAKAO, K., AND SAKAE, T. (2006): Status of the parametric X-ray generator at LEBRA, Nihon University, *Nuclear Instr. Methods in Physics Res*, **B**, (in press)

[6] BELLUCCI S. AND BIRYUKOV V. (2006): The future looks bright for particle channelling, *CERN COURIER,* **46**, pp. 37-38

[7] SUGA, S. AND GUSTAFSON, G. (1963): Studies on the development of rat enamel by means of histochemistry, microradiography, and polarized light microscopy, *Proc 9th ORCA Cong Dent Caries, Paris,* pp. 223-244

[8] SAKAE T. AND HIRAI G. (1982): Calcification and crystallization in bovine enamel, *J.Dent.Res.* **61**, pp. 57-59

Pit Formation in Human Enamel and Dentin Irradiated using the 2.94 μm LEBRA-Free Electron Laser

Toshiro Sakae, Yukie Sato, Yasuhiro Tanimoto, Masanori Higa, Hirokazu Oinuma, Yukishige Kozawa, Hiroyuki Okada, Hirotsugu Yamamoto, Toru Hayakawa, Kimiya Nemoto, Takeshi Sakai, Kyoko Nogami, Akira Mori, Takao Kuwada, Yasushi Hayakawa, Toshinari Tanaka, Ken Hayakawa, and Isamu Sato

IJOMS Volume 4 Number 1 May 2005

International Journal of Oral-Medical Sciences

Research Institute of Oral Science

Int J Oral-Med Sci 4(1):8-13, 2005

Original Article

Pit Formation in Human Enamel and Dentin Irradiated using the 2.94 μm LEBRA-Free Electron Laser

Toshiro Sakae,[1] Yukie Sato,[2] Yasuhiro Tanimoto,[3] Masanori Higa,[1] Hirokazu Oinuma,[1] Yukishige Kozawa,[1] Hiroyuki Okada,[2] Hirotsugu Yamamoto,[2] Toru Hayakawa,[3] Kimiya Nemoto,[3] Takeshi Sakai,[4] Kyoko Nogami,[4] Akira Mori,[4] Takao Kuwada,[4] Yasushi Hayakawa,[4] Toshinari Tanaka,[4] Ken Hayakawa,[4] and Isamu Sato[4]

Departments of [1]Histology, Cytology and Developmental Anatomy, [2]Oral Pathology, and [3]Dental Biomaterials, Nihon University School of Dentistry at Matsudo, Matsudo, Chiba, 271-8587, Japan
[4]LEBRA, Laboratory for Electron Beam Research and Application, Institute of Quantum Science, Nihon University, Funabashi, Chiba, 274-8501, Japan

Correspondence to :
Toshiro Sakae
E-mail : sakae@mascat.nihon-u.ac.jp

Abstract
The ablation effect of laser treatment of dental tissues is mainly determined by : i) wavelength, ii) power fluence, and iii) pulse structure. To evaluate the effect of pulse structure, the 2.94 μm free electron laser (FEL) and the Er:YAG laser were used to irradiate human tooth enamel and dentin. A 2.94 μm FEL of 8-10 μsec excision with 2 Hz was generated by the 80 MeV LINAC-undulater system at LEBRA, Nihon University, with the macro-pulse structure of 20 μsec and with less than 1 pico-second micro-pulses at 350 pico-sec interval. Size and depth of the pits formed by laser irradiation were measured using a profilometer. Only a 3 mJ LEBRA-FEL was sufficient to form a crater in the enamel and dentin, and the depth of the pit formed by laser irradiation was dependent upon the power of laser. Even when the higher-powered FEL was applied, the craters showed no signs of scorching. Conversely, craters with scorching were evident when the Er : YAG laser was used on dentin. In conclusion, heat damage of dental hard tissues can be avoided using a micro-pulse structured laser.

Keywords :
enamel, dentin, FEL, pit

Introduction

Laser use in dentistry has grown dramatically during the past two decades. Potential applications include for detection of dental caries lesion (1), aesthetic dentistry (2), dental implantology (3), periodontology (4, 5), endodontics (6), dental calculus and caries removal (7), hardening of tooth surface (8), gingival contouring, bleaching, frenectomy, treatment for hypersensitivity (9, 10). The use of lasers in the dental field has been proclaimed by several researchers (11, 12, 13), and the benefits are widely recognized (14, 15).

For excavation of dental enamel and dentin, the laser wavelength generally selected is 2.94 μm (the Er:YAG laser), since absorbance by water in the tissues is maximum at this wavelength. Laser ablation effects are mainly influenced by wavelength, power-fluence, and pulse structure. Thus, the effect of pulse structure can be determined using lasers with the same wavelength and similar power energy for irradiation experiment.

Lasers used in the clinical and experimental field are usually solid-crystal generated and EXCIMA lasers, both of which operate at a fixed wavelength. The free electron laser (FEL) has a wavelength that is adjustable, spanning wavelengths from a millimeter, to visible and potentially ultraviolet, to x-ray. It can exhibit the optical properties characteristic of conventional lasers, such as high spatial coherence, and a near diffraction limited radiation beam. It

differs from conventional lasers in that it uses a relativistic electron beam as its lasing medium, as opposed to bound atomic or molecular states. Using these FEL characteristics, the Laboratory for Electron Beam Research and Application (LEBRA) at Nihon University used the LINAC-system to develop the LEBRA-FEL. This laser has a 20 μsec macro-pulse/less than 1 pico-sec micro-pulse structure.

The aim of this study was to compare the ablation effect of LEBRA-FEL and Er:YAG, lasing with different pulse structures, on dental enamel and dentin.

Materials and Methods

Tooth Preparation

Three human molar teeth, preserved in 10% neutral formaldehyde solution, were used in this study. They had been extracted prior to the establishment of the committee for Ethics at Nihon University School of Dentistry. These teeth sectioned using a low speed diamond saw (Buhler, USA).

Free Electron Laser (FEL) Irradiation

The principles of generating FEL using linac and undulater has been previously described (16, 17). For the LEBRA-LINAC FEL system, the electron beam is pulsed at 2 Hz, and the laser is on for 20 microseconds, depending on the wavelength and the "tune". This long pulse of several microseconds is generally referred to as the macropulse. The macropulse of electrons comprise a train of very short micropulses, less than 1 picosecond long, and these micropulses are spaced by the timing of the RF oscillations (350 picoseconds). The electron beam is introduced into an undulater, which is composed of a series of magnets. The electron beam is oscillated by these magnets but the light passes through linearly and reflects between by two mirrors to resonate and amplify (Fig. 1).

The LEBRA-FEL was operated under the following conditions - accelerating voltage of 80 MeV; macro-pulse of 20 μsec, 2 Hz; Micro-pulse of 70 mA, less than 1 pico-second with a 350 pico-second interval; Undulater gap interval of 15.0 mm; FEL

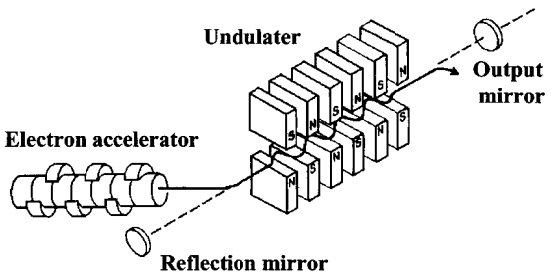

Fig. 1. Principle of generating FEL.

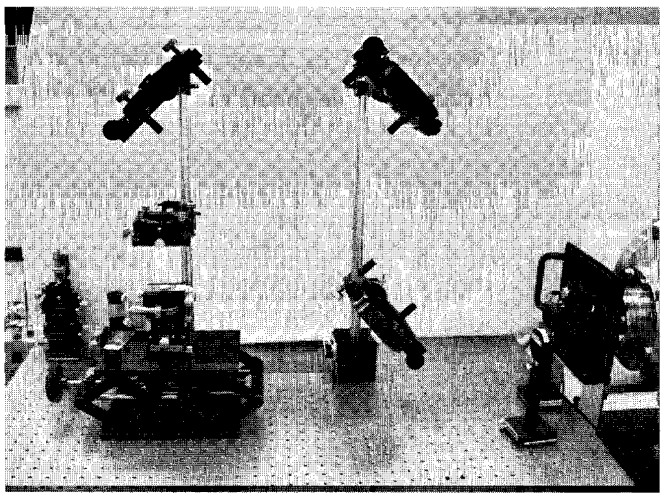

Fig. 2. FEL irradiation equipment.
The FEL passed along the vacuumed tube from the undulater and came out through the calcium fluoride windows at the right side of the photo, reflected by three mirrors, then passed a condenser lens, CaF_2, f=100 mm, to focus on the surface of sample which was placed horizontally.

wavelength of 2.94 μm; FEL excision of 8-10 μsec. The irradiating energy was regulated by a diaphragm through which the laser light passed. The power of irradiation was monitored before and after irradiation of the sample, and there was 15% fluctuation of power. The FEL was used to irradiate the section for an exposure time of 1 to 3 macro-pulse shots. Fig. 2 shows the FEL irradiation equipment used. The tooth section was mounted into the sample holder to permit irradiation at the right angle to the sample.

Er:YAG Laser Irradiation

An Er:YAG laser irradiation instrument for experimental use (HOYA PHOTONICS Co. Ltd., Tokyo) was also used in this study. The experimental conditions were as follows - output wavelength of 2.94

μm ; cycle of 3 Hz ; output power of 350 mJ ; transmission using a fiber ; irradiation tip of quartz. The irradiation was carried out at the same laboratory room as to the LEBRA-FEL irradiation.

Measurements of the Pits formed by the Laser Irradiation

The lased teeth sections were observed under a binocular microscopy (NIKON, Tokyo), and images were recorded on a digital camera. The size and depth of the pits formed by laser irradiation were measured using a surface profilometer (VF-7500, KEYENCE, Osaka).

Results

An example of a LEBRA-FEL irradiated human tooth is shown in Fig. 3. On irradiation, there was a glint of light blue color and a faint smell akin to that of drilled dentin. After irradiating, pits or craters on both the enamel and dentin surface were visible with the naked eyes. The ablation effect of the LEBRA-FEL appeared to be related to the dose of irradiation. Using the same dose of irradiation, dentin was excavated deeper than enamel. Table 1 shows the depth of pits measured using a surface profilometer. Pits had a crater-like or conical appearance.

The depth of the pits formed by irradiation with the LEBRA-FEL appeared dose dependent, when the unfitted data from 16 μm to 99 μm for enamel and from 17 μm to 111 μm for dentin was excluded (Fig. 4). The width of the pits were dependent upon the dose of irradiation but the relation coefficient was not clear from 129 μm to 174 μm for enamel and from 40 μm to 192 μm for dentin. In some cases, irradiation spots were visible at the enamel-dentin junction, where pit depth and width were between those for enamel and dentin (Table 1).

Fig. 5. shows another example of LEBRA-FEL irradiation of human enamel and dentin. Again, the pits formed by the irradiation appeared to be dose dependent. There was no sign of scorching of enamel or dentin at any dose of irradiation used in this experiment. By contrast, irradiation with the Er: YAG laser resulted in scorching of the surface of pits (Fig. 6).

Discussion

The FEL has a number of attributes not seen with the solid-state laser system and EXCIMA lasers, for example in terms of arbitrary tunable wavelengths that are resonantly absorbed by phosphates, proteins, and water (18, 19). In general, a shorter period laser irradiation resulted in the less thermal damage of the dental tissues. Some investigators limit thermal damages using a Q-switched nano-second micro -pulsed Er:YAG laser instead of a free-running laser (20).

This study focused on the effect of pulse structure

Table 1. Depth and width of the pits formed by irradiation of LEBRA-FEL in enamel and dentin.

HE position	1 Enamel	2 Enamel	3 Dentin	4 Dentin	5 Dentin	6 Dentin	7 Dentin	8 Dentin	9 Dentin	10 Dentin	11 Dentin
irradiation shot	6	6	5	5	4	4	3	3	2	2	1
depth	99	85	90	88	83	85	98	94	52	62	16
width	157	152	159	179	153	181	127	122	103	103	40
TE position	1 Enamel	2 EDJ	3 Dentin	4 Dentin	5 Dentin	6 Dentin	7 EDJ	8 Enamel	9 Enamel	10 Enamel	
irradiation shot	2	2	3	3	3	3	2	2	1	1	
depth	31	78	111	97	92	103	81	33	18	17	
width	174	131	192	137	150	163	179	156	137	129	

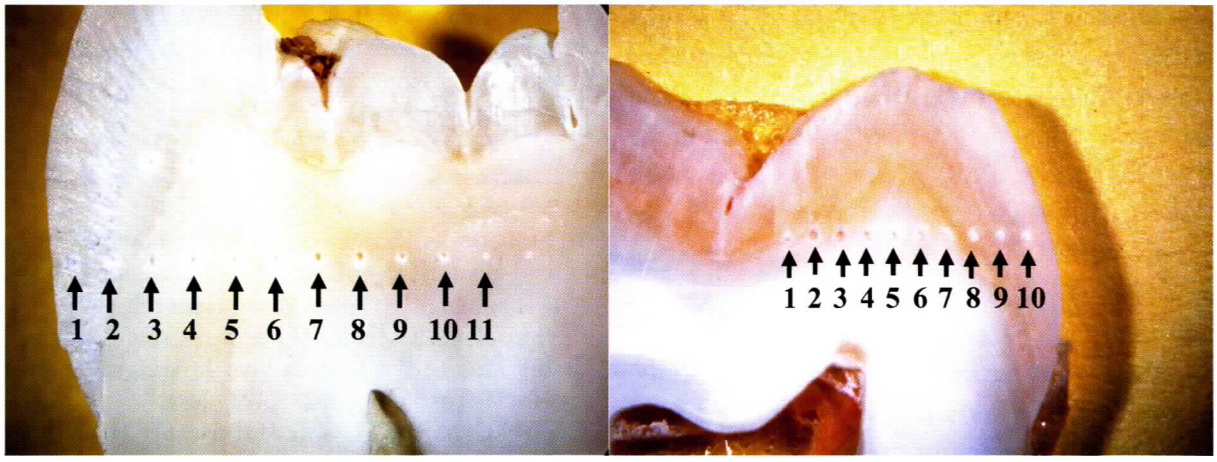

Fig. 3. FEL irradiated human tooth samples, left (HE) and right (TE).
See Table 1 for the details.

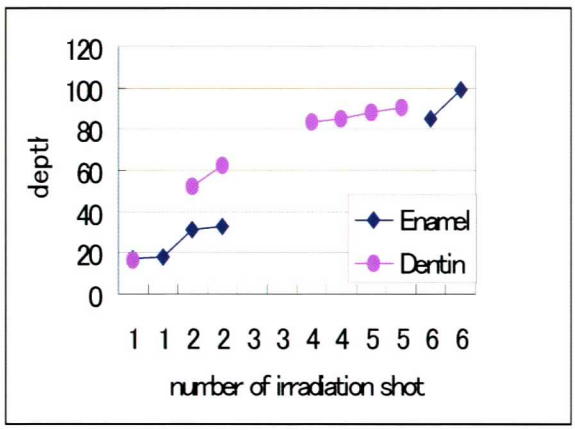

Fig. 4. Plots of irradiation pit depth of human enamel and dentin vs number of irradiation shot. Data are listed in Table 1. Shot number of 3 were omitted because of these deviations.

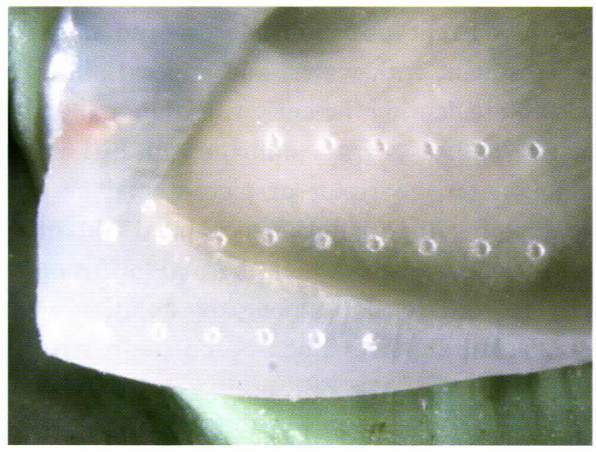

Fig. 5. FEL irradiated human tooth.
Numbers of the irradiation shot were 1, 1, 2, 2, 3 and 3, from the left to right, respectively, for the dentin (the top series) ; 1, 1, 1, 1, 1, 2, 2, 3 and 3, from the left to right, respectively, for the enamel and dentin (the middle series) ; and 1, 1, 2, 2, 3, and 3, from the left to right, respectively, for the enamel (the bottom series).

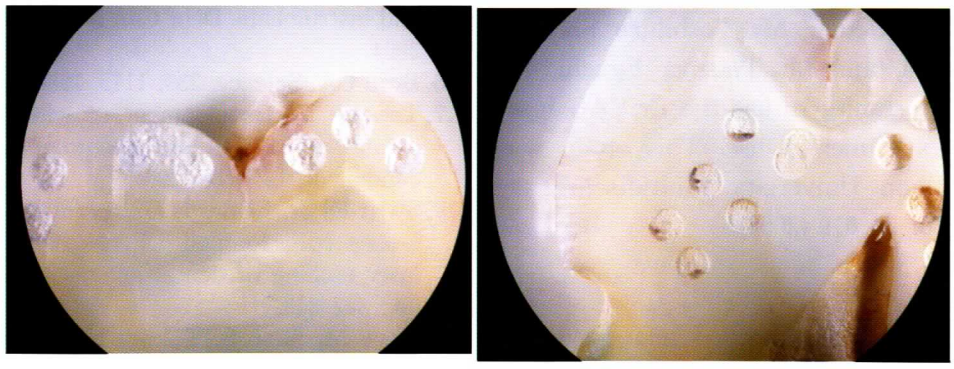

Fig. 6. Er:YAG laser irradiation on human tooth enamel (left) and dentin (right).
The irradiation, power of 350 mJ, was carried out with water for the right three spots on the enamel (left) and without for the left four spots on the enamel, and without water for the left three lined sopts on the dentin. Scorching was observed in the irradiated pits on dentin.

of the laser on tooth enamel and dentin. The results showed that the thermal damage resulting from user of the laser differed between the LEBRA-FEL and Er:YAG lasers. When the Er:YAG laser is used in the dental setting, water is used for cooling so as to avoid thermal damage (21). In a recent study, Er: YAG laser irradiation resulted in the enamel heating to 1600 °C (22). The irradiation of dental enamel with subablative erbium laser irradiation produces fine cracks in the enamel surface (8). In the current study, unlike with the LEBRA-FEL, use of the Er:YAG laser resulted in scorching of dentin.

The short pulse structure of infrared lasers result in less thermal damage than that associated with lasers in current use. Sub-microsecond pulsed IR lasers resonant with water, and mineral absorption bands ablate dentin efficiently with minimal thermal damage (23). Less thermal damage with FEL irradiation might be the result of pico-second or nano-second pulses that induce mechanical ablation of tooth structure faster than thermal diffusion. To clarify the relationship among the ablation effects, pulse structure, power fluence and tooth structure, further study with the FEL are necessary.

Acknowledgments

This study was carried out using the FEL system equipped at the LINAC of LEBRA, Nihon University. LEBRA-FEL is one of the projects considered an Academic Frontier Project from the MEXT, Japan. The authors thank HOYA PHOTONICS Co. Ltd., Tokyo, in particular Mr. Toshihiro Shibata, Mr. Yasuharu Sato, and Mr. Tetsuya Eguchi, for providing the opportunity to use the Er:YAG laser instrument for experimental use. This study was supported by Nihon University Multidisciplinary Research Grant for 04-019 (2004).

References

1. Featherstone JD: Caries detection and prevention with laser energy. Dent Clin North Am, 44 (4), 955-969, 2000.
2. Adams TC, Pang PK: Lasers in aesthetic dentistry. Dent Clin North Am, 48 (4), 833-860, 2004.
3. Martin E: Lasers in dental implantology. Dent Clin North Am, 48 (4), 999-1015, 2004.
4. Ishikawa I, Aoki A, Takasaki AA: Potential application of Erbium: YAG laser in periodontics. J Periodontal Res, 39 (4), 275-285, 2004.
5. Mavrogiannis M, Thomason JM, Seymour RA: Lasers in periodontology. Dent Update, 31 (9), 535-538, 541-542, 545-547, 2004.
6. Stabholz A, Sahar-Helft S, Moshonov J: Lasers in endodontics. Dent Clin North Am, 48 (4), 809-832, 2004.
7. Rechmann P: Dental laser research: selective ablation of caries, calculus, and microbial plaque: from the idea to the first in vivo investigation. Dent Clin North Am, 48 (4), 1077-1104, 2004.
8. Apel C, Meister J, Gotz H, Duschner H, Gutknecht N: Structural changes in human dental enamel after subablation erbium laser irradiation and its potential use for caries prevention. Caries Res, 39 (1), 65-70, 2005.
9. Stabholz A, Zeltser R, Sela M, Peretz B, Moshonoz J, Ziskind D, Stabholz A: The use of lasers in dentistry: principles of operation and clinical applications. Compend Contin Educ Dent, 24 (12), 935-948, 2003.
10. Walsh LJ: The current status of laser application in dentistry. Aust Dent J, 48 (3), 146-155, 2003.
11. Convissar RA: The biological rationale for the use of lasers in dentistry. Dent Clin North Am, 48 (4), 771-794, 2004.
12. Dederich DN, Bushick RD, ADA Council on Scientific Affairs and Division of Science; Journal of the American Dental Association: Lasers in dentistry: separating science from hype. J Am Dent Assoc, 135 (2), 204-212, 2004.
13. Myers TD, Sulewski JG: Evaluation dental lasers: what the clinical should know. Dent Clin North Am, 48 (4), 1127-1144, 2004.
14. van As G: Erbium lasers in dentistry. Dent Clin North Am, 48 (4), 1017-1059, 2004.
15. Coluzzi DJ: Fundamentals of dental lasers: science and instruments. Dent Clin North Am, 48 (4), 751-770, 2004.
16. Brau CA, Science, 239, 1115, 1988.
17. Tanaka T: Development of wide band coupled undulater at LEBRA. www.lebra.nihon-u.ac.jp/pdf/ws/2undul.pdf, LEBRA, 2000
18. Swift EJ Jr, Edwards GS, Perdigao J, Thompson JY, Nunes MF, Ruddell DE, Negishi A: Free-electron laser etching of dental enamel. J Dent. 2001 Jul; 29 (5): 347-353.
19. Heya M, Sano S, Takagi N, Fukami Y, Awazu K: Wavelength and average power density dependency of the surface modification of root dentin using an MIR-FEL. Lasers Surg Med. 2003; 32 (5): 349-358.
20. Khabbaz MG, Makropoulou MI, Serafetinides AA, Papadopoulos D, Papagiakoumou E: Q-switched ver-

sus free-running Er:YAG laser efficacy on the root canal walls of human teeth : a SEM study. J Endod. 2004 Aug ; 30 (8) : 585-588.
21. Hossain M, Nakamura Y, Yamada Y, Kimura Y, Nakamura G, Matsumoto K : Ablation depths and morphological changes in human enamel and dentin after Er:YAG laser irradiation with or without water mist. J Clin Laser Med Surg. 1999 Jun ; 17 (3) : 105-109.
22. Hirota F : Annual Meeting Japanese Association for Oral Bilogy, Abstract No., 2004.
23. Dela Rosa A, Sarma AV, Le CQ, Jones RS, Fried D : Peripheral thermal and mechanical damage to dentin with microsecond and sub-microsecond 9.6 microm, 2.79 microm, and 0.355 microm laser pulses. Lasers Surg Med. 2004 ; 35 (3) : 214-228.

Ann Anat 189 (2007) 175–181

Available online at www.sciencedirect.com
ScienceDirect

ANNALS OF ANATOMY
www.elsevier.de/aanat

Effect of fluoride ions on apatite crystal formation in rat hard tissues

M. Kakei[a,*], T. Sakae[b], M. Yoshikawa[c], N. Tamura[d]

[a]*Division of Oral Anatomy, Meikai University School of Dentistry, 1-1 Keyakidai, Sakado, Saitama 350-0283, Japan*
[b]*Department of Histology, Cell Biology, and Embryology, Nihon University School of Dentistry at Matsudo, 2-870-1 Sakaechyo-nishi, Matsudo, Chiba 271-003-61, Japan*
[c]*Division of Orthodontics, Meikai University School of Dentistry, 1-1 Keyakidai, Sakado, Saitama 350-0283, Japan*
[d]*Division of Chemistry, Meikai University School of Dentistry, 1-1 Keyakidai, Sakado, Saitama 350-0283, Japan*

Received 15 June 2006; accepted 25 July 2006

KEYWORDS
Fluoride;
Carbonic anhydrase;
Central dark line;
Crystal abnormality;
Electron microscopy

Summary

Fluoride is widely believed to be a useful chemical substance for preventing dental caries. However, the mechanism underlying crystal perforation in the tooth enamel and the effect of fluoride on hard tissues are unclear. To clarify the mechanism of the biological action of fluoride in the mineralization process, we examined the hard tissues of rats having received water containing a relatively low fluoride level. Electron microscopy revealed that fluoride ions could interrupt the crystal nucleation process, resulting in crystal perforation in the developing tooth enamel and the presence of amorphous minerals in bone crystals. Furthermore, the results of enzymatic analyses indicated that fluoride directly interfered with the synthesis of carbonic anhydrase by the enamel-forming cells, rather than being directly involved in the crystal formation. From the results, we would like to provide a possible mechanism of crystal perforation in the enamel induced by fluoride intake. Also, we would like to suggest that regardless of its amount, fluoride intake has harmful effects on both tooth and bone formation.

Introduction

In dentistry, a variety of fluoride-containing products are being employed because fluoride use is believed to be a preventive measure against tooth decay (McCann and Bullock, 1957; Zipkin et al., 1960; Larson et al., 1976; Arends and Christoffersen, 1990; Colquhoun, 1993; Featherstone, 1999; Petersen and Lennon, 2004). Fluoride is also used for the treatment of osteoporosis in the medical faculty (Rich and Ensinck, 1961; Farley et al., 1987; Boivin et al., 1988; Fratzl et al., 1994,

*Corresponding author. Tel.: +81 492 85 5511; fax: +81 492 87 6657.
E-mail address: m-kakei@dent.meikai.ac.jp (M. Kakei).

0940-9602/$ - see front matter © 2006 Elsevier GmbH. All rights reserved.
doi:10.1016/j.aanat.2006.07.009

1996). Although numerous studies on fluoride have reported their beneficial effects such as caries prevention (McCann and Bullock, 1957; Zipkin et al., 1960; Larson et al., 1976; Arends and Christoffersen, 1990; Colquhoun, 1993; Featherstone, 1999; Petersen and Lennon, 2004), as well as harmful effects such as dental and skeletal fluorosis (Fejerskov et al., 1979; Ando et al., 1998, 2001; Sampaio et al., 1999; Choubisa et al., 2001), the effects of fluoride on hard tissues remain controversial (Faccini, 1969; Diesendorf, 1986; Riggs et al., 1987; Denbesten, 1999). Crystal perforation has been reported to occur in fluorosed human dental enamel (Kerebel and Daculsi, 1976; Yanagisawa et al., 1989). Crystal perforation in the enamel has revealed the absence of the central dark line, which is known as the nucleation site of apatite crystals (Marshall and Lawless, 1981; Nakahara, 1982; Nakahara and Kakei, 1984, 1989; Kakei, 1989; Kakei and Nakahara, 1996; Kakei et al., 1997, 2005). With regard to the central dark line in apatite crystals, our recent study has clarified that the physical properties of the central dark line are different from those of octacalcium phosphate (Kakei et al., 2005), which is considered as a candidate mineral for the central dark line (Brown et al., 1962, 1987; Nelson and Mclean, 1984; Nelson and Barry, 1989). In addition, it is thought that both carbonate and magnesium ions may contribute to the formation of the central dark line (Casciani et al., 1979; Kakei et al., 1997). Therefore, we conducted this study to clarify the mechanism underlying crystal perforation based on our assumption that the crystal nucleation process might be hampered by fluoride intake. To determine whether fluoride directly affects crystal formation, we analyzed the carbonic anhydrase, which is thought to mainly provide the carbonate ions in the mineral component of hard tissues, in the developing rat enamel matrix, because this enzyme might directly supply carbonate ions for initiating the crystal nucleation process in the calcification of hard tissues (Nakahara and Kakei, 1984, 1989; Kakei, 1989; Kakei and Nakahara, 1996; Kakei et al., 1997).

In our present electron microscopic study, we mainly examined the mechanism by which fluoride affects the crystallization process in the tooth enamel and external table of the calvaria.

Materials and methods

Experimental animal

The experimental group comprised male Sprague-Dawley rats (3 wks of age) that were given free access to drinking water, containing 0.1, 0.3 or 0.5 mg/l fluoride ions for 12 wks. The hard tissues of these animals were subjected to electron microscopy and chemical analysis. To demonstrate the crystal perforation in the enamel, we provided water containing up to 2.0 mg/l fluoride to an additional group. The control rats were provided water that did not contain fluoride. Samples were excised from anesthetized rats. For electron microscopy, the samples were dissected into small sections, and the calvariae were cut perpendicular to the surface. The fluoride-affected regions in developing rat incisors and bone were determined in advance based on the results of tetracycline labeling. The enamel matrix proteins from rat incisors were prepared for western blotting and for determining the carbonic anhydrase activity. The use of animals was approved by the Animal Care and Use Committee of Meikai University.

Transmission electron microscopy

The samples were fixed in 2% glutaraldehyde in 0.1 M cacodylate buffer at pH 7.4 for 1 h at 5 °C, post-fixed with 1% osmium tetroxide in the same buffer for 2 h at 5 °C, dehydrated by passage through a series of ascending ethanol concentrations and embedded in Araldite 502. Thin sections were obtained using an ultramicrotome equipped with a diamond knife. The sections were floated on the water saturated with crystal minerals. Unstained sections and those stained with uranyl acetate and lead citrate were examined under a JEM 100CX at an accelerating voltage of 80 kV.

Biochemical analyses of carbonic anhydrase

After removal of the adhering blood and surrounding soft tissues, the incisors were rinsed with a cold saline solution. The immature enamel materials obtained from 8 wk-old animals consisting of the early (matrix formation) and middle (transitional) stages of enamel development, were scraped from the incisors. Each sample (3.0 mg; wet weight) of the developing enamel materials was homogenized in 150 µl electrophoretic sample buffer. In each group, equal amounts of protein (30 µg) were subjected to electrophoresis. After electrophoretic blotting on a nitrocellulose membrane (BA 85; Schleicher & Schuell, Dassel, Germany), amido black staining and immunological detection were conducted on the membrane. Anti-carbonic anhydrase antibodies were prepared as described previously (Kakei, 1989). Electrophoretic blotting and the immunological detection of

carbonic anhydrase on the nitrocellulose membrane were conducted by the method of Towbin et al. (1979). Enzymatic activity was measured using the pH change method of Wilbur and Anderson (1948) with some modifications. Each sample of the developing enamel tissues was lyophilized, pulverized and then suspended in distilled water. A 0.3-ml aliquot of the suspension containing 3.0 mg enamel powder was tested for enzymatic activity. The reaction solution for the measurement of enzymatic activity contained 6.0 ml of 0.02 M Veronal buffer; this solution was adjusted to pH 8.2 at 0 °C. The tissue suspension (0.3 ml) was added to the solution. Next, 5 ml CO_2-saturated cold water was introduced into the mixture using a syringe. The time interval required to lower the pH from 8.0 to 6.3 was measured. For the controls, 0.3 ml distilled water was used instead of the tissue suspension. Values are mean ± standard deviation (S.D.) of 3–5 experiments. The enzymatic activity was expressed as a pH time course.

Results

During the 12-wk experimental period, the body weight of rats in all groups increased from approximately 50–550 g. No significant differences were recognized between the experimental and control groups with regard to the general condition.

Mineralization began simultaneously with the protein secretion from Tomes' processes of ameloblasts at the secretory stage of the developing rat enamel (Fig. 1a). Despite the disappearance of Tomes' processes at the maturation stage, the growth process of the crystals continued until they attained full maturity (Fig. 1b). Observation of the stained and unstained sections revealed that the ribbon-shaped elements of the enamel that are initially formed adjacent to Tomes' processes consisted of 2 components—an electron-dense thin outer organic layer (the organic envelope; Fig. 1c) and a relatively electron-lucent inner precursor mineral (Fig. 1d). The first line represented the crystal nucleation site within the organic envelope (Fig. 1e). Crystal growth was recognized as an increase in the number of lattice lines along the first dense line (Fig. 1f). Possibly, the first line persisted in the mature crystal (data not shown). Based on our findings, we present schematics (Figs. 1g–i) depicting crystal formation from the nucleation stage to the maturation stage. Similarly, in bones, needle-shaped elements, which possessed an envelope structure similar to that observed in

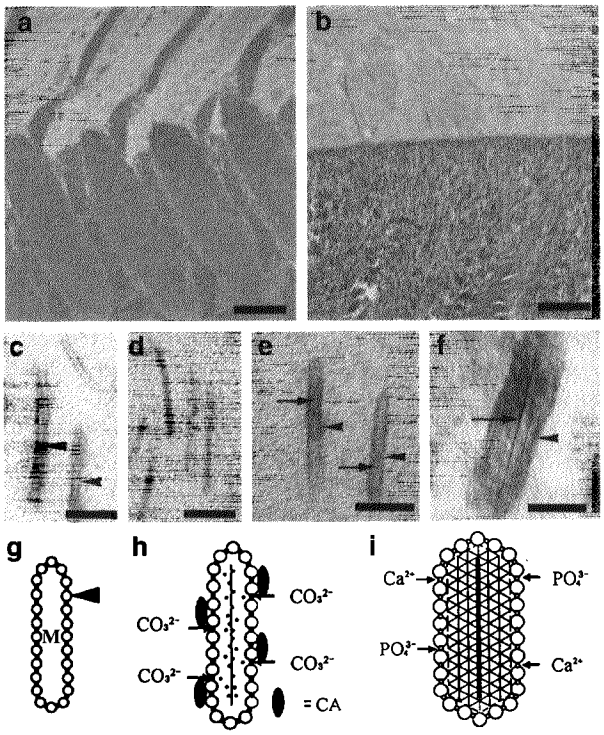

Figure 1. Electron micrographs of the crystal formation process in the enamel (a)–(f) and schematics (g)–(i). (a) Secretory stage of the developing rat enamel. Early ribbon-shaped elements and Tomes' processes (asterisks) of ameloblasts. (b) Maturation stage of the developing rat enamel. (c) Cross-section of the ribbon-shaped element at the early stage. (d) Precursor mineral within the envelope structure at the early stage. (e) Central dark line first appears within the envelope structure. (f) Developing enamel crystal. (g) Schematics of the envelope structure and precursor minerals (M), consisting of calcium, phosphate and magnesium ions, based on photos "c" and "d". (h) Crystal nucleation by carbonic anhydrase (CA) corresponding to photo "e". Dots indicate the magnesium carbonate salt. (i) Crystal growth corresponding to photo "f". Carbonate ions might serve to neutralize the inhibitory effect of magnesium ions by forming a magnesium carbonate salt for initiating the nucleation process. Subsequently, crystal nucleation occurs in the presence of both activated calcium and phosphate ions. Arrowheads, envelope structure; arrows, central dark line. Scale bars: 30 μm (a) and (b), 10 nm (c)–(f). Stained sections (a)–(c), (e) and (f); non-stained section (d).

the enamel, were located at the calcification front, and the crystal growth proceeded towards the advancing front (data not shown).

Electron micrographs of enamel crystals at the secretory stage revealed that the immature crystals showing lack of lattice images seemed to be more abundant in the experimental animals than in the control animals (Fig. 2a). However, in this study, we obtained crucial evidence regarding the

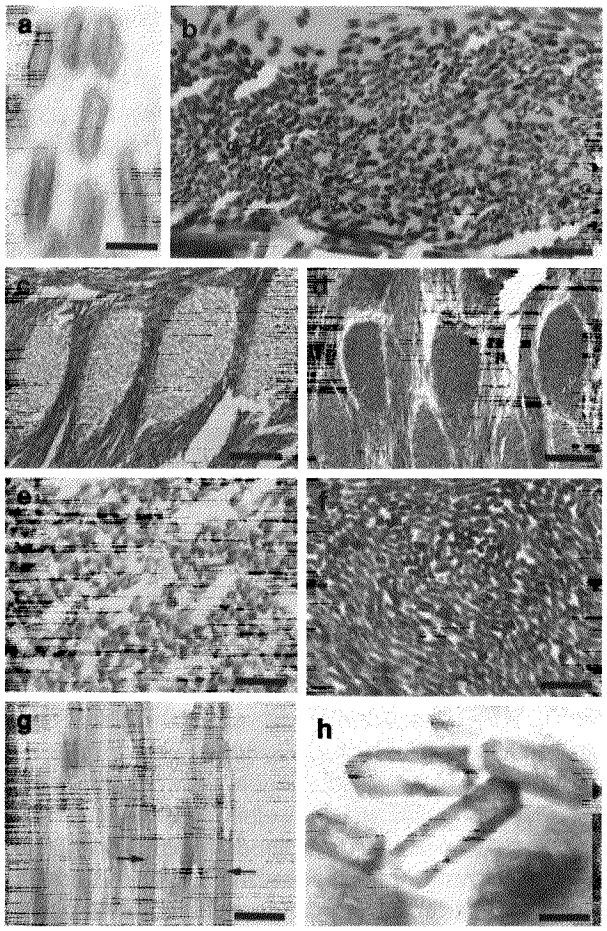

Figure 2. Electron micrographs of fluoride-affected crystals (a)–(c), (e), (g) and (h) and normal crystals (d) and (f) in the enamel. (a) Cross-section of the fluoride-affected immature crystals. (b) A small number of perforated crystals at the maturation stage. (c) Fluoride-affected enamel rods at low magnification. (d) Enamel rods of the controls at low magnification. (e) A fluoride-affected enamel rod at high magnification. (f) An enamel rod of the control group at high magnification. (g) Longitudinal sections of the fluoride-affected enamel. (h) Cross-section of perforated crystals. Arrows indicate the central dark lines. 0.5-mg/l group (a) and (b), 2.0-mg/l group (c), (e), (g) and (h) and control group (d) and (f). Scale bars: 20 nm (a), 200 nm (b), 2 μm (c) and (d), 200 nm (e) and (f), 50 nm (g), 20 nm (h). Stained sections (a); non-stained sections (b)–(h).

presence of a small number of perforated crystals among the crystals obtained from rats in the 0.5-mg/l fluoride group (Fig. 2b). These crystals had central perforations and were observed at the maturation stage of the enamel (Fig. 2b). Next, we examined the rats that received fluoride at a considerably higher level, i.e. 2.0 mg/l. At lower magnification, many enamel rods were sparsely filled with crystals; at high magnification, the enamel rods consisted of crystal fragments and/or perforated crystals when compared with the control crystals (Figs. 2c–h). However, crystal perforation was not detected in bones; a large number of fine, dense crystals were observed at the maturation sites without any visible abnormality at low magnification (Fig. 3a). However, at high magnification, a number of crystals lacked the lattice lines within the envelope structures in the stained sections (Fig. 3b). Additionally, the unstained sections showed an amorphous mineral with a fuzzy (or unclear) structure; this structure was different from that of the control crystals (Figs. 3c and d).

Next, we analyzed the key enzyme—carbonic anhydrase—in the developing enamel matrix, although the electrophoretic patterns suggested that fluoride might have affected the synthesis of some matrix proteins (Fig. 4a). Using an anti-rat carbonic anhydrase antibody for western blot analysis, it was clearly demonstrated that the quantity of this enzyme, which is secreted by ameloblasts, was remarkably reduced in the 0.5-mg/l fluoride group (Fig. 4b). In addition, the

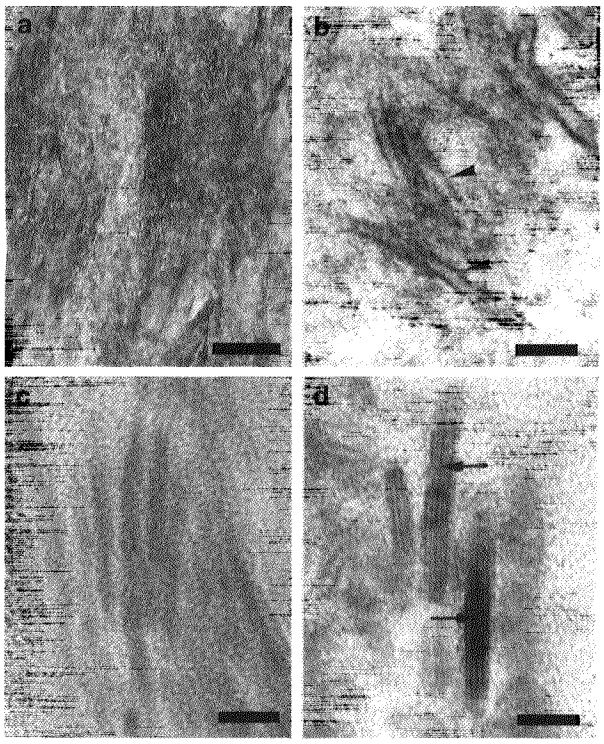

Figure 3. Electron micrographs of fluoride-affected bone crystals (a)–(c) and normal crystals (d). (a) Fluoride-affected bone crystals at low magnification. (b) Stained section showing envelope structures. (c) Non-stained section showing amorphous minerals. Arrowheads, envelope structure; arrows, central dark line. (a)–(c) 0.5-mg/l group; (d) control group. (d) Bone crystals of the control group. Scale bars: 100 nm (a) and 10 nm (b)–(d). Stained sections (a) and (b); non-stained sections (c) and (d).

carbonic anhydrase activity in the developing enamel matrix tended to decline with an increase in the fluoride levels (Fig. 4c).

Discussion

It is generally believed that the central area of the apatite crystal, which includes the central dark line, may contain a higher concentration of both carbonate and magnesium ions (Boyde, 1979; Quint et al., 1980; Kakei et al., 1997). Furthermore, magnesium ions are assumed to inhibit the crystal nucleation process at the early stage of crystal formation (LeGeros, 1981). Taking into consideration these reports together with our notion regarding the crystal nucleation process (Kakei, 1989; Nakahara and Kakei, 1989; Kakei and Nakahara, 1996; Kakei et al., 1997), it is plausible that carbonate ions might serve to neutralize the inhibitory effect of magnesium ions by forming a magnesium carbonate salt for initiating the nucleation process (Casciani et al., 1979; Kakei et al., 1997). Regarding the crystal perforation in the enamel, although some researchers have reported that fluorosed human dental enamel is accompanied by crystal perforation, they concluded that this phenomenon might have resulted from dental decay (Kerebel and Daculsi, 1976; Yanagisawa et al., 1989). In the present study, however, we have observed such perforated crystals in the developing enamel of unerupted rat teeth. Based on the results obtained from the present study, we have presented an explanation of the mechanism of crystal perforation in the enamel (Figs. 5a–c). Under conditions of the influence of fluoride, analysis of the longitudinal sections of crystals in Fig. 2g revealed that even if the carbonic anhydrase supply from the ameloblasts stops due to the presence of fluoride, crystallization would occur continuously towards the *c*-axis at the peripheral area (Fig. 5b), whereas the central area would remain amorphous (Fig. 5c). This is because the central area is considered to be influenced by magnesium ions. Eventually, observation of the cross-sections of crystals (Fig. 2(h) revealed a central perforation in Fig. 5c. However, crystal perforation may not occur in bone crystals because of the lack of the crystal nucleation

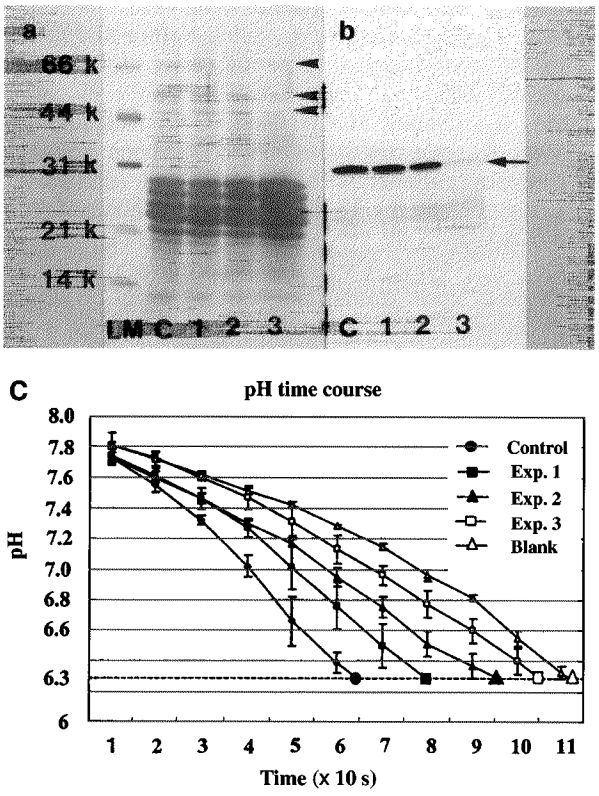

Figure 4. Effect of fluoride on the carbonic anhydrase activity in the developing enamel matrix. (a) Electrophoretic patterns obtained from each sample. Some matrix proteins (arrowheads) in the 0.5-mg/l group (lane 3) are affected by fluoride intake. (b) Western blot analysis showing a reduction in carbonic anhydrase (arrow) in the 0.5-mg/l group (lane 3). (c) Enzymatic activities at different fluoride concentrations. LM, low molecular weight standard; C, sample from control group animals; Exp.1, 0.1-mg/l; Exp. 2, 0.3-mg/l; Exp. 3, 0.5-mg/l group animals and Blank, blank test without enamel matrix. Error bars indicate S.D.

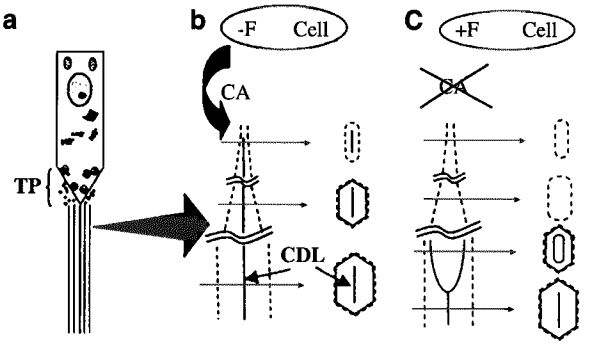

Figure 5. Schematics of the crystal perforation process in the enamel crystal (a)–(c). (a) Tomes' process (Tp) of an ameloblast and ribbon-shaped elements (long parallel lines). (b) Enlarged ribbon-shaped element. In the controls, ameloblasts supply carbonic anhydrase (CA) for initiating the nucleation process. (c) After the nucleation stops, crystallization continues to occur at the periphery area. CDL, central dark line. Left side: longitudinal sections of the ribbon-shaped elements; right side: cross-sections corresponding to each region indicated by arrows. Broken lines indicate organic envelopes.

process. In addition, we expect that the crystal perforation may also reduce transparency of enamel crystals and partially account for the white spots observed on fluorosed human dental enamel (Kerebel and Daculsi, 1976; Yanagisawa et al., 1989).

To date, the effect of low fluoride concentration on the carbonic anhydrase activity has rarely been reported, and crystal damage is barely seen at a low fluoride level. However, we conclude that even a low level fluoride would interfere with the synthesis of this enzyme whose action might inevitably initiate the nucleation process (Kakei, 1989; Nakahara and Kakei, 1989; Kakei and Nakahara, 1996; Kakei et al., 1997). Therefore, we believe that fluoride may directly affect hard tissue-forming cells, which are responsible for synthesizing carbonic anhydrase and secreting it into the extracellular matrix for initiating the crystal nucleation process, rather than being directly involved in crystal formation. The crystal nucleation process is likely to be hampered significantly due to an insufficient supply of carbonate ions, thereby resulting in the presence of amorphous minerals in bone crystals and crystal perforation in enamel crystals. This may explain why fluoride intake results in a decrease in carbonate and a slightly higher content of magnesium ions in the mineral component of hard tissues (McCann and Bullock, 1957; Zipkin et al., 1960).

Here, we strongly suggest that even small amounts of fluoride may indirectly affect crystal formation by directly affecting the carbonic anhydrase synthesis in hard tissue-forming cells, although various fluoridation schemes that aim at preventing dental caries are employed and recommended by many countries and organizations as well as by the World Health Organization (Petersen and Lennon, 2004). In addition, our recent findings clearly demonstrated that the crystal structure of the enamel surface is not modified by a simple treatment with fluoride agents, which are widely used in dental clinics, and show that fluoride ions remain on the enamel surface, indicating that the effectiveness of fluoride is very doubtful (personal communication). We expect unnecessary fluoride intake to affect the crystal formation during the critical tooth and bone development stages, although a structural damage in hard tissues is barely seen at a low fluoride level. We believe that excess fluoride intake might lead to more serious dental and skeletal fluorosis (Ando et al., 1998; 2001; Sampaio et al., 1999; Choubisa et al., 2001). Furthermore, we speculate that fluoride therapy for osteoporosis might have an adverse effect.

Acknowledgements

This work was supported by the Frontier Science Promotion Program at the Laboratory for Electron Beam Research and Application (LEBRA), Nihon University, Japan.

References

Ando, M., Tadano, M., Asanuma, S., Tamura, K., Matsushima, S., Watanabe, T., Kondo, T., Sakurai, S., Ji, R., Liang, C., Cao, S., 1998. Health effects of indoor fluoride pollution from coal burning in China. Environ. Health Perspect. 106, 239–244.

Ando, M., Tadano, M., Yamamoto, S., Tamura, K., Asanuma, S., Watanabe, T., Kondo, T., Sakurai, S., Ji, R., Liang, C., Chen, X., Hong, Z., Cao, S., 2001. Health effects of fluoride pollution caused by coal burning. Sci. Total Environ. 271, 107–116.

Arends, J., Christoffersen, J., 1990. Nature and role of loosely bound fluoride in dental caries. J. Dent. Res. 69, 601–605.

Boivin, G., Chapuy, M.-C., Baud, C.A., Meunier, P.J., 1988. Fluoride content in human iliac bone: results in controls, patients with fluorosis, and osteoporotic patients treated with fluoride. J. Bone Miner. Res. 3, 497–502.

Boyde, A., 1979. Carbonate concentration, crystal centers, core dissolution, caries, cross striations, circadian rhythms, and compositional contrast in the SEM. J. Dent. Res. 58, 981–983.

Brown, W.E., Smith, J.P., Lehr, J.R., Frazier, A.W., 1962. Octacalcium phosphate and hydroxyapatite. Nature 196, 1048–1054.

Brown, W.E., Eidelman, N., Tomazic, B., 1987. Octacalcium phosphate as a precursor in biomineral formation. Adv. Dent. Res. 1, 306–313.

Casciani, F.S., Etz, E.S., Newbury, D.E., Doty, S.B., 1979. Raman microprobe studies of two mineralizing tissues: enamel of the rat incisor and the embryonic chick tibia. Scan. Electron Microsc. 2, 383–391.

Choubisa, S.L., Choubisa, L., Choubisa, D.K., 2001. Endemic fluorosis in Rajasthan. Indian J. Environ. Health 43, 177–189.

Colquhoun, J., 1993. Fluorides and the decline in tooth decay in New Zealand. Fluoride 26, 125–134.

Denbesten, P.K., 1999. Biological mechanisms of dental fluorosis relevant to the use of fluoride supplements. Community Dent. Oral Epidemiol. 27, 41–47.

Diesendorf, M., 1986. The mystery of declining tooth decay. Nature 322, 125–129.

Faccini, J.M., 1969. Fluoride and bone. Calci. Tissue Res. 3, 1–16.

Farley, S.M.G., Wergedal, J.E., Smith, L.C., Lundy, M.W., Farley, J.R., Baylink, D.J., 1987. Fluoride therapy for osteoporosis: characterization of the skeletal response by serial measurements of serum alkaline phosphatase activity. Metabolism 36, 211–218.

Featherstone, J.D.B., 1999. Prevention and reversal of dental caries: role of low level fluoride. Community Dent. Oral Epidemiol. 27, 31–40.

Fejerskov, O., Yaeger, J.A., Thylstrup, A., 1979. Microradiography of the effect of acute and chronic administration of fluoride on human and rat dentine and enamel. Arch. Oral Biol. 24, 123–130.

Fratzl, P., Roschger, P., Eschberger, J., Abendroth, B., Klsushofer, K., 1994. Abnormal bone mineralization after fluoride treatment in osteoporosis: a small-angle X-ray scattering study. J. Bone Miner. Res. 10, 1541–1549.

Fratzl, P., Schreiber, S., Roschger, P., Lafage, M-H., Rodan, G., Klsushofer, K., 1996. Effects of sodium fluoride and alendronate on the bone mineral in minipigs: a small-angle X-ray scattering and back-scattered electron imaging study. J. Bone Miner. Res. 11, 248–253.

Kerebel, B., Daculsi, G., 1976. Ultrastructurale et cristallographique de l'émail human dans la fluorose endémique. J. Biol. Bucccale 4, 143–154.

Kakei, M., 1989. The role of carbonic anhydrase in mineralization process of rat hard tissues. Thesis, Tokyo Metropolitan University.

Kakei, M., Nakahara, H., 1996. Aspects of carbonic anhydrase and carbonate content during mineralization of the rat enamel. Biochim. Biophys. Acta 1289, 226–230.

Kakei, M., Nakahara, H., Tamura, N., Itoh, H., Kumegawa, M., 1997. Behavior of carbonate and magnesium ions in the initial crystallites at the early developmental stages of the rat calvaria. Ann. Anat. 179, 311–316.

Kakei, M., Sakae, T., Yoshikawa, M., Tamura, N., 2005. Physical properties of the central dark lines in biological apatite of vertebrate calcified tissues and synthetic octacalcium phosphate. J. Fossil Res. 38, 43–48.

Larson, R.H., Mellberg, J.R., Englander, H.R., Senning, R., 1976. Caries inhibition in the rat by water-borne and enamel-bound fluoride. Caries Res. 10, 321–331.

LeGeros, R.Z., 1981. Apatites in biological system. Prog. Crystal Growth Charact. 4, 1–45.

Marshall, A.F., Lawless, K.P., 1981. TEM study of the central dark line in enamel crystallites. J. Dent. Res. 60, 1773–1782.

McCann, H.G., Bullock, F.A., 1957. The effect of fluoride ingestion on the composition and solubility of mineralized tissues in the rat. J. Dent. Res. 36, 391–398.

Nakahara, H., 1982. Electron microscopic studies of the lattice image and 'central dark line' of crystallites in sound and carious human dentin. Josai Shika Daigaku Kiyo 11, 209–215.

Nakahara, H., Kakei, M., 1984. TEM observations on the crystallites of dentin and bone. Josai Shika Daigaku Kiyo 13, 259–263.

Nakahara, H., Kakei, M., 1989. Central dark line and carbonic anhydrase: problems relating to crystal nucleation in enamel. In: Fearnhead, R.W., Suga, S. (Eds.), Tooth Enamel 4. Elsevier, Amsterdam, pp. 42–46.

Nelson, D.G.A., Barry, J.C., 1989. High resolution electron microscopy of nonstoichiometric apatite crystals. Anat. Rec. 224, 265–276.

Nelson, D.G.A., Mclean, D., 1984. High-resolution electron microscopy of octacalcium phosphate and its hydrolysis products. Calcif. Tissue Int. 36, 219–232.

Petersen, P.E., Lennon, M.A., 2004. Effective use of fluorides for the prevention of dental caries in the 21st century: the WHO approach. Community Dent. Oral Epidemiol. 32, 319–321.

Quint, P., Althoff, J., Hohling, H.J., Boyde, A., Laabs, W.A., 1980. Characteristic molar ratios of magnesium, carbon dioxide, calcium and phosphorus in the mineralizing fracture callus and predentine. Calcif. Tissue Int. 32, 257–261.

Rich, C., Ensinck, J., 1961. Effect of sodium fluoride on calcium metabolism in human beings. Nature 1991, 184–185.

Riggs, B.L., Baylink, D.J., Kleerekoper, M., Lane, J.M., Melton III., L.J., Meunier, P.J., 1987. Incidence of hip fractures in osteoporotic women treated with sodium fluoride. J. Bone Miner. Res. 2, 123–126.

Sampaio, F.C., von der Fehr, F.R., Arneberg, P., Gigante, D.G., Hatløy, A., 1999. Dental fluororsis and nutritional status of 6- to 11-year-old children living in rural areas of Paraiba, Brazil. Caries Res. 33, 66–73.

Towbin, H., Staehelin, T., Gorolon, J., 1979. Electrophoretic transfer of proteins from polyacrylamide gels to nitrocellulose sheets: procedure and some applications. Proc. Natl. Acad. Sci. USA 79, 4350.

Wilbur, K.M., Anderson, N.G., 1948. Electrometric and colorimetric determination of carbonic anhydrase. J. Biol. Chem. 176, 147–154.

Yanagisawa, T., Takuma, S., Tohda, H., Fejerskov, O., Fearnhead, W., 1989. High resolution electron microscopy of enamel crystals in cases of human dental fluorosis. J. Electron Microsc. 38, 441–448.

Zipkin, I., McClure, F.J., Lee, W.A., 1960. Relation of the fluoride content of human bone to its chemical composition. Arch. Oral Biol. 2, 190–195.